Phase I Final Report

DESIGN OF A
DUAL PATCH MULTI-ELEMENT
RADIANT COOLER

R. V. Annable and J. F. Lodder

ITT Aerospace/Optical Division
Electro-Optical Operations
Fort Wayne, Indiana 46803

July 1970

Design Study Report for Period 16 February to 16 July 1970

Prepared for

GODDARD SPACE FLIGHT CENTER
Greenbelt, Maryland 20771

1. Report No.	2. Government Accession No.	3. Recipient's Catalog No
4. Title and Subtitle DESIGN OF A DUAL PATCH MULTI-ELEMENT RADIANT COOLER		5. Report Date July 1970 6. Performing Organization Code
7. Author(s) R. V. Annable and J. F. Lodder		8. Performing Organization Report No
9. Performing Organization Name and Address ITT Aerospace/Optical Division Electro-Optical Operations Fort Wayne, Indiana 46803		10. Work Unit No 11. Contract or Grant No NAS5-21132 13. Type of Report and Period Covered Design Study
12. Sponsoring Agency Name and Address Goddard Space Flight Center Greenbelt, Maryland 20771 I. L. Goldberg, Code 731		14. Sponsoring Agency Code
15. Supplementary Notes		

16. Abstract

PREFACE

This report covers the thermal and mechanical design of a dual patch multi-element radiant cooler for earth oriented applications. The cooler is designed to attain temperatures of 120K and 90K in a circular 9:30 AM orbit at an altitude of 450 n mi. The patches are designed to accommodate a 14 element InAs array at 120K and a 4 element HgCdTe array at 90K. The report includes a thermal analysis for the specified orbit and a plan for testing the cooler. The designs studied show a direct trade-off between low patch temperatures and small cooler dimensions. Variations in thermal properties show that temperatures are most sensitive to changes in the emissivity of the low-emissivity surfaces within the cooler.

17. Key Words	18. Distribution Statement		
19. Security Classif. (of this report)	20. Security Classif. (of this page)	21. No. of Pages	22. Price

PREFACE

This report covers the thermal and mechanical design of a dual patch multi-element radiant cooler for earth oriented applications. The cooler is designed to attain temperatures of 120K and 90K in a circular 9:30 AM orbit at an altitude of 450 n mi. The patches are designed to accommodate a 14 element InAs array at 120K and a 4 element HgCdTe array at 90K. The report includes a thermal analysis for the specified orbit and a plan for testing the cooler. The designs studied show a direct trade-off between low patch temperatures and small cooler dimensions. Variations in thermal properties show that temperatures are most sensitive to changes in the emissivity of the low-emissivity surfaces within the cooler.

TABLE OF CONTENTS

LIST OF ILLUSTRATIONS

LIST OF TABLES

LIST OF TABLES (Continued)

1.0 INTRODUCTION

This report covers the thermal and mechanical design of a dual patch multi-element radiant cooler for earth oriented applications. The nominal dual patch temperatures are 120K and 90K at an instrument housing temperature of 300K. The thermal inputs produced by the introduction of the detectors are equivalent to a 14 element InAs array at 120K and a 4 element HgCdTe array at 90K. The report includes the calculation of patch temperatures for the specified orbit and the description of a plan for testing the cooler.

The cooler is designed for operation on an earth-oriented spacecraft in a circular sun-synchronous orbit at an altitude of 450 n mi and an orbit normal to sun angle of 52.5 degrees (9:30 AM orbit). The cooler is mounted on the anti-solar side of the orbital plane, where it is shaded from direct sunlight.

The basic conditions and requirements imposed on the dual patch multi-element radiant cooler were established and a basic cooler design formulated (Section 2.0). The exact dimensions were then determined for a range of cooler designs that meet the imposed conditions. Four of these were selected for detailed thermal analysis (Sections 3.0 and 4.0). The analysis is based on the specular image array technique (Section 5.0). The detailed mechanical design of one of the four selected coolers (which has patches and cone in common with another design) was then carried out (Section 6.0). Finally, a plan was devised for testing this specific cooler in a space chamber under realistic thermal conditions (Section 7.0).

The limiting dimension of the cooler is its linear extent parallel to the intersection of the orbital and horizontal planes, called the length. Two nominal lengths, 12 and 14 inches, were studied. The nominal length does not include the cooler extension in the form of an earth shield. A modified 12 inch size was also considered, in which the length including the earth shield was restricted to 12 inches.

All the selected designs have calculated first patch temperatures well below the nominal 120K. All designs also achieve the second patch value (90K) or below at an instrument temperature of 25 degrees C even in the presence of degraded thermal properties. However, the modified 12 inch design fails to attain the nominal temperature when the degraded properties are combined with the maximum housing temperature of 50 degrees C.

The cooler consists of two high-emissivity patches whose emission is directed to cold regions of space by means of a low-emissivity, specular cone. The cone, in turn, is cooled by an attached high-emissivity surface (cone end) not visible from the patches. The view from the cone end is also restricted to cold space, in this case by a low-emissivity, specular shield at the temperature of the instrument housing.

Increasing the cooler size from 12 to 14 inches has little influence on the cone temperature. On the other hand, reducing the size of the shield (by modification of the nominal 12-inch size) significantly increases the cone temperature. This is largely the result of the reduced cone end area rather than the reduced shielding from the earth. Maximizing the patch area within a given nominal size does little to change the temperatures of the patches. Otherwise, there is a reciprocal relationship between patch temperature and physical size. The thermal performance improves with an increase in the nominal size and in the shield size.

Variations in thermal properties show that the temperature of the first (120K) patch is most sensitive to changes in the infrared emissivity of the low-emissivity surfaces (cone and shield walls). Second in its effect on patch temperature is the shielding of the multilayer insulation between the housing and cone and between the cone and patch. The temperature of the second (90K) patch is also relatively sensitive to changes in the detector thermal input (joule heat and radiation from the optical opening) and in its conductive coupling to the first patch.

An attempt was made to improve the performance of the second patch by transferring area to it from the first patch. This was possible because the calculated temperature of the first patch was well below the nominal 120K value under all conditions. However, the resultant change was either a small reduction or, in a few cases, even a small increase. We must therefore conclude that improved performance by means of an increased patch area can be obtained in this case only by increasing the size of the entire cooler.

The cooler will employ means to prevent thermal and optical degradation produced by condensed water vapor or other outgassed products. To this end, the design includes a cone cover to postpone or terminate cooling action (Section 6.2) and anti-frost enclosures to prevent condensation on the optical opening at the patch (Section 6.3 and Appendix A). Other methods of preventing or eliminating the condensation of volatiles within a radiant cooler are described in Section 8.0 of the Design Study Report on Contract NAS5-21112 (Surface Compensation Mapping Radiometer for the Nimbus E Spacecraft, Feb. 4 - May 4, 1970, ITT Aerospace/ Optical Division for Goddard SFC).

2.0 BASIC DESIGN

It is assumed that the radiant cooler has a rectangular geometry in which the patch normal (cone axis) lies in a vertical plane through the centers of the patch and earth but is rotated an angle ψ above the horizontal (plane through the patch center parallel to the tangent plane at the satellite subpoint). It is further assumed that the cone mouth lies in a vertical plane whose normal is at an angle ψ with the patch normal and whose surface is parallel with the orbital plane. The cross-section of the cone perpendicular to the patch normal is then a rectangule, and the cone mouth is a trapezoid.

The radiant cooler is subject to the conditions or constraints imposed by the orbit and spacecraft. These conditions can, in general, be translated into requirements on the design of the radiant cooler. The basic conditions are those imposed by the orbit:

1. Circular orbit at an altitude of 450 n mi.

2. Orbit normal to sun angle of 52.5 degrees (9:30 AM orbit).

The first condition limits the view to cold space because of the region occupied by the earth and its atmosphere. At an altitude of 450 n mi, the tangent line to the earth's atmosphere at the equator (earth radius of 3444.3 n mi and atmospheric height of 9.1 n mi) is 27 degrees 47 minutes below the horizontal. Reducing this angle to provide margins for spacecraft wobble and instrument alignment, the first condition was translated into the following requirement:

a. Maximum view angle to cold space in the vertical plane through the centers of the patch and earth of 26 degrees below the horizontal (i.e., in the direction of the nadir).

A small region of the hemisphere above the cone mouth in the zenith direction may be occupied by spacecraft instrumentation such as a horizon sensor. We will assume that the view factor from a cooler patch to such instrumentation is very small and that the resultant increase in patch temperature is negligible.

However, if the cooler is not mounted on a spacecraft of rectangular geometry (such as the ITOS) but on a spacecraft of circular geometry (such as the Nimbus), the view to cold space may be further restricted. Mounting restrictions may result in an upward view to the bottom of the spacecraft. The design would then be modified for the reduced view to cold space and the view from the cone mouth to the spacecraft restricted or eliminated by a shield.

It is also assumed that the cooler is mounted on the shaded side of the spacecraft (anti-solar side of the orbital plane), so that there is no direct sunlight on the cooler and no cooler requirements corresponding to orbital condition 2.

Additional requirements are imposed by the spacecraft and available space:

b. Base temperature of 25 degrees C ± 25 degrees C.

c. Maximum cooler dimensions as follows:

Vertical (Height)	12 inches
Length* (In plane of cone mouth)	12, 14 inches
Depth (Perpendicular to cone mouth)	12 inches
Extension from plane of cone mouth (Away from spacecraft)	6 inches

* Exclusive of cooler extension (earth shield).

d. Cone mouth at the edge of the spacecraft.

Two lengths, 12 and 14 inches, will be considered. In addition, a design will be studied in which the overall length including the extension beyond the edge of the spacecraft is restricted to 12 inches. The extension (earth shield) has been limited to 6 inches. It forms part of a deployable cone cover (Section 6.0).

The following requirement was imposed in order to keep the cone-patch radiative coupling at a low value. It is possible to meet it because of the large view to space available in three directions.

e. The first reflection of the cone mouth in each cone wall has one boundary in or below the plane of the patch.

Under this condition, no more than two cone wall reflections are needed for a patch ray to reach cold space. It therefore also simplifies the analysis of the cone-patch radiative interchange.

The best choice of ψ (maximum view to cold space) is the maximum angle subtended from the cone mouth by the earth and its atmosphere (64^{o}). In this case, the cone has only three walls, as shown by the typical basic design in Figure 1. In order to meet conditions a and e, the back wall of the cooler must make an angle of 0^{o} or larger with the patch normal. To meet condition e, the side walls must make a minimum angle with the patch normal given by

$$\sin 2\theta_p = \ell_c/a, \tag{1}$$

where ℓ_c = maximum height of the cone measured normal to the patch

a = maximum length of the cone mouth (i.e., its dimension at the top).

Two cooler design ranges were developed, as shown in Tables 1 and 2. These correspond to cooler lengths of 12 and 14 inches, respectively, exclusive of the earth shield. A design with an overall length of 12 inches including the earth shield was obtained by modifying the design selected for analysis from Table 1. The basic design and dimensions of the radiant cooler are illustrated in Figure 1. The nomenclature is as follows:

w_p = width of patch opening

ℓ_p = length of patch opening

w_d = width of cone end

ℓ_d = length of cone end

ℓ_c = length of cone

ℓ_m = length of cone mouth

h_m = height of cone mouth

ℓ_s = length of shield

ℓ_o = length of shield mouth

θ_c = angle of cone side walls

θ_s = angle of shield side walls

A_{po} = area of patch opening

A_m = area of cone mouth

A_d = area of cone end

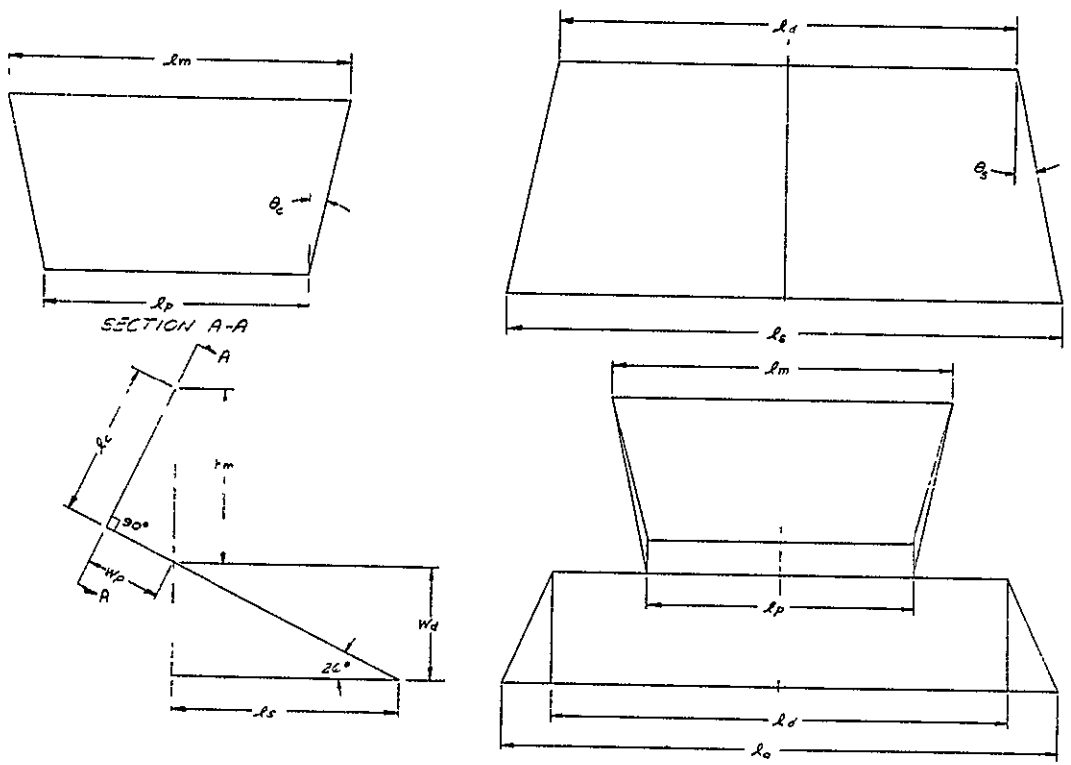

Figure 1 Basic Design of Multi-Element Radiant Cooler

Table 1 Range of 12-Inch Cooler Designs

w_p	ℓ_p	A_{po}	ℓ_c	h_m	A_m	A_d/A_m	θ_c(°)
2.0	7.023	14.046	4.101	4.562	36.55	0.961	13.55
2.1	6.806	14.293	4.306	4.791	37.86	0.927	14.29
2.2	6.576	14.467	4.511	5.019	39.09	0.898	15.04
2.3	6.331	14.561	4.716	5.247	40.22	0.873	15.80
2.4	6.071	14.570	4.921	5.475	40.50	0.867	16.57
2.5	5.795	14.4875	5.126	5.703	42.19	0.832	17.36
2.6	5.502	14.305	5.331	5.931	43.01	0.816	18.16
2.7	5.192	14.018	5.536	6.159	43.70	0.803	18.98
3.0	4.140	12.420	6.151	6.844	44.965	0.781	21.56
3.5	1.864	6.524	7.176	7.984	58.58	0.599	26.44
*3.5394	1.646	5.826	7.257	8.074	42.98	0.817	26.87
3.8015	0	0					

* Maximum patch width

Linear dimensions in inches; areas in square inches.

Table 2 Range of 14-Inch Cooler Designs

w_p	ℓ_p	A_{po}	ℓ_c	h_m	A_m	A_d/A_m	θ_c (°)
2.0	9.414	18.828	4.101	4.562	46.56	0.880	10.94
2.1	9.244	19.412	4.306	4.791	48.49	0.845	11.52
2.2	9.065	19.943	4.511	5.019	50.35	0.8135	12.11
2.3	8.876	20.415	4.716	5.247	52.14	0.786	12.69
2.4	8.676	20.822	4.921	5.475	53.86	0.760	13.29
2.5	8.465	21.1625	5.126	5.703	55.50	0.738	13.89
2.6	8.244	21.434	5.331	5.931	57.07	0.718	14.49
2.7	8.011	21.630	5.536	6.159	58.54	0.700	15.11
2.8	7.766	21.745	5.741	6.387	59.93	0.683	15.73
2.9	7.509	21.776	5.946	6.615	61.22	0.669	16.36
3.0	7.239	21.717	6.151	6.844	62.41	0.656	17.00
3.1	6.956	21.564	6.356	7.072	63.49	0.645	17.65
3.2	6.658	21.306	6.561	7.300	64.45	0.6335	18.31
3.3	6.346	20.942	6.766	7.528	65.29	0.627	18.98
3.4	6.018	20.461	6.971	7.756	66.00	0.621	19.66
3.5	5.674	19.859	7.176	7.984	66.57	0.615	20.36
*3.5394	5.531	19.576	7.257	8.074	66.74	0.614	20.65
3.6	5.312	19.123	7.381	8.212	66.98	0.6115	21.07
4.0	3.662	14.648	8.201	9.125	66.90	0.612	24.10
4.5	0.980	4.410	9.226	10.265	61.49	0.666	28.50
4.6463	0	9	9.526	10.599	25.55	-	30.00

* Maximum patch width

Linear dimensions in inches; areas in square inches.

Both design ranges have a minimum patch opening width of 2 inches. The cone end area for the designs in Table 1 is 35.11 in^2 and in Table 2, 40.96 in^2. There is a maximum patch width set by the maximum cooler height of 12 inches. The values shown in the tables allow 1 inch for structure, so that the maximum value of $w_d + h_m$ is 11 inches. In addition, there are extreme values of the cone length and patch width at which the patch length goes to zero as a result of the imposed conditions (condition e for a given value of ℓ_m). These extremes are given by

$$\ell_{cx} = \frac{\sqrt{3}}{2} \ell_m \tag{2}$$

and

$$w_{px} = 0.48773\, \ell_{cx} \tag{3}$$

A condition corresponding to e was also applied to the design of the shield.

f. The first reflection of the shield mouth in each shield wall has one boundary in or below the plane of the cone end.

The main portion of the shield (horizontal wall) was set at 90 degrees to the plane of the cone end. To meet condition f, the side walls must then make a minimum angle θ_s with the cone end normal given by

$$\tan \theta_s = \frac{-1 + \sqrt{3K^2 + 1}}{3K}, \tag{4}$$

where $K = \ell_s/\ell_d$. The length of the shield mouth is then given by

$$\ell_o = \ell_d + 2\, \ell_s \tan \theta_s,$$

$$\ell_o = \frac{1}{3}\left(\ell_d + 2\sqrt{\ell^2_d + 3\,\ell^2_s}\right) \tag{5}$$

The following designs were selected for detailed thermal analysis:

Design	w_p	ℓ_p	ℓ_m	ℓ_c	w_d	ℓ_d	ℓ_s	ℓ_o
IA	2.0	7.023	9	4.101	2.926	12	6	14.583
IIA	2.0	9.414	11	4.101	2.926	14	6	16.290
IIB	3.0	7.239	11	6.151	2.926	14	6	16.290
IIIA	2.0	7.023	9	4.101	2.926	8.785	6	12

Design IA was selected from Table 1. It has the minimum patch opening width w_p of 2 inches. There is little change in the area of the opening A_{po} (< 4%) as w_p goes from 2 inches to 2.7 inches, where A_{po} has its maximum value. The design with the minimum w_p was therefore selected in order to obtain the minimum value of ℓ_c and A_m (and therefore maximum A_d/A_m). In addition, the earth shielding of the cone mouth is a maximum for this design.

Design IIA and IIB were selected from Table 2. The former has the minimum patch width and the latter a near maximum patch opening. These choices permit a study of the trade-offs as the patch width is increased. For example, Design IIB has an A_{po} value about 15 percent larger than IIA but an A_d/A_m ratio about 25 percent smaller.

Design IIIA has the same patch-cone geometry as IA. However, the earth shield has been modified (with a resultant reduction in the cone end area A_d) in order to limit the overall cooler length to 12 inches.

3.0 CONE TEMPERATURE RANGES

The steady-state thermal balance equation of the cone is

$$\epsilon_d \sigma T_c^4 = H_e + H_h + H_i + H_k \qquad (6)$$

where ϵ_d = emissivity of cone end

T_c = cone temperature

H = radiant incidence

e = earth

h = shield

i = multilayer insulation

K = supports and electrical leads

This equation neglects the cone mouth absorption of shield (infrared) radiation and the cone mouth emission of (infrared) radiation. These are small and tend to offset each other. In addition, the shield is assumed to be at the temperature of the instrument housing.

The equivalent infrared exitance of the earth can be obtained by equating the power emitted by the earth to that absorbed from the sun. The result is

$$W_e = (1/4) S_o (1 - A) = 2.1 \times 10^{-2} \text{ W} \cdot \text{cm}^{-2} \qquad (7)$$

where S_o is the solar constant (0.14 W $\cdot$ cm^{-2}) and A the average albedo of the earth (0.4). Also, the reflected sunlight exitance of the earth averaged over an orbit is

$$W_r = (1/\pi) S_o A \cos\beta_s = 1.78 \times 10^{-2} \cos\beta_s \text{ W} \cdot \text{cm}^{-2} \qquad (8)$$

where β_s is the solar elevation angle above the orbital plane. This is the reflected solar exitance seen from a near-earth orbit and can be obtained from the formula in Appendix I to Part I of the Final Report on Contract No. NAS5-10113 (December 1967) as the limiting value when the nadir to earth tangent line angle, $\pi/2 - \vartheta_o$, approaches $\pi/2$.

The radiant incidence from the earth is then

$$H_e = \left(\alpha_{me} W_r + \epsilon_{me} W_e\right) \frac{A_m}{A_d} \quad (9)$$

where α_{me} = cone mouth absorptivity for earth reflected sunlight

ϵ_{me} = cone mouth absorptivity for earth emitted infrared

A_m/A_d = ratio of cone mouth area to cone end area (Section 2.0).

The thermal response time of the cone is large compared with a near-earth orbital period, so that the cone responds to the average values of earth exitance. The view to earth from the cone end is blocked by the shield at or above the minimum spacecraft altitude of 450 n mi. The radiant incidence from the shield is

$$H_h = \epsilon_d \, a_{dh} \, \sigma T_h^4 \quad (10)$$

where a_{dh} = effective emissivity of the shield as seen from the cone end

T_h = shield (instrument housing) temperature

The effective absorptivities and emissivities needed to calculate the radiative inputs to the cone mouth and cone end are given in Section 5.0.

The input through the multilayer insulation may be considered entirely radiative (it is, in fact, a complex combination of radiative and conductive). The interchange between the housing and outer cone surface (wall and end) is reduced by the shielding factor s_i of the insulation,

$$H_i = \frac{\sigma A_i}{s_i A_d} \left(T_h^4 - T_c^4\right), \quad (11)$$

where A_i is the area of the outer cone surface (Table 3).

Table 3 Cone Surface Areas

Design	A_i	A_d
IA	167	35.11
IIA	202	40.96
IIB	209	40.96
IIIA	158	25.70

All in square inches

The radiant incidence equivalent to conduction through the supports and electrical leads to the cone is

$$H_k = \frac{K_c}{A_d} (T_h - T_c), \quad (12)$$

where K_c is the thermal conductance. The connections between the housing and cone are listed in Table 4. The resultant thermal conductance is

$$K_c = 1.317 \times 10^{-3} \text{ W} \cdot \text{K}^{-1}$$

Table 4 Connections Between Housing and Cone

Quantity	to	dia (inch)	material	k*
15	InAs array	3.3×10^{-3}	chromel	0.13
5	HgCdTe array	5.0×10^{-3}	nickel	0.78
2	cone temp. meas.	3.3×10^{-3}	chromel	0.13
4	patch temp. meas.	3.3×10^{-3}	chromel	0.13
2	cone heater	5.2×10^{-3}	chromel	0.13
4	patch heaters	3.3×10^{-3}	chromel	0.13
6	supports	1/4 x 3/16	synthane	3.3×10^{-3}

* Thermal conductivity in W/cm · K
All connections are 1 inch in length.

The cone temperatures of the four selected designs (Section 2.0) were first calculated for the following set of nominal radiative properties.

α_c = solar absorptivity of cone wall = 0.13 (aluminum)

ϵ_c = infrared absorptivity of cone wall = 0.05

ϵ_h = infrared emissivity of shield = 0.05

ϵ_d = infrared emissivity of cone end = 1

S_i = shielding factor of cone insulation = 100

The resultant cone temperatures are listed in Table 5 for three values of housing temperature T_h and the difference among the designs shown in Table 6. Increasing the cooler size from a nominal 12 inches to 14 inches (Tables 1 and 2, Section 2.0) has little influence on the cone temperature (designs IA and IIA). On the other hand, reducing the size of the shield significantly increases the cone temperature. This is shown by a comparison of design IIB with IIA (14-inch design) and of design IIIA with IA (reduction in shield length to restrict maximum cooler dimension to 12 inches). A variation in housing temperature of ± 25 degrees C about 25 degrees C changes the cone temperature by approximately ± 11K.

Next, the surface thermal properties were degraded from the nominal values in order to study their influence on the cone temperature. First, the solar absorptivity of the cone walls α_c was increased by a factor of 1.69 x to 0.22, a value representative of a gold surface. Secondly, the infrared absorptivity of the cone wall ϵ_c and the emissivity of the shield ϵ_h were increased to 0.07, a factor of 1.40X. Thirdly, the shielding factor of the insulation S_i was reduced to 80, a degradation of 1.25X. And finally, all three thermal properties were degraded at the same time. The results are listed in Tables 7 to 10, which show both the cone temperatures and their increases from the nominal values.

The lowest cone temperatures are attained in all cases by design IIA. However, the performance of the smaller IA is nearly as good. The highest temperatures are attained by design IIIA. Because its cone design is the same as that of IA, the increases must result from the reduction in shield length (Section 2.0). Design IIB has intermediate values of cone temperature. However, it is the most sensitive to changes in the thermal parameters. Design IA is least sensitive to changes, but only slightly less than design IIA and IIIA. On the basis of cone design alone, the best choice is therefore design IA.

The values of radiant incidence (referred to the cone end) of design IIIA are listed in Table 11 for the nominal (Table 5) and maximum (Table 10) cone temperatures. The corresponding housing temperature is 25 degrees C in both cases. It is seen that the input from the earth is relatively small although this design has the smallest shield. The larger cone temperatures compared with those of design IA (which has the same cone) must therefore be largely the result of the reduced cone end area. The (earth) power absorbed by the cone walls is 0.067 W in the nominal case and 0.106 W in the maximum.

Table 5 Cone Temperatures for Nominal Radiative Properties

Design	T_c for T_h equal to 0°C	25°C	50°C
IA	152.6	163.6	174.9
IIA	152.0	163.1	174.5
IIB	155.0	165.7	176.9
IIIA	160.8	172.1	183.8

Temperatures in Kelvins

Table 6 Cone Temperature Differences from Design IIA

Design	Increase in T_c for T_h equal to 0°C	25°C	50°C
IA	0.6	0.5	0.4
IIA	0	0	0
IIB	3.0	2.6	2.4
IIIA	8.8	9.0	9.3

Temperatures in Kelvins

Table 7 Cone Temperatures for α_c Equal to 0.22

T_c for T_h equal to

Design	0°C	25°C	50°C
IA	154.0	164.7	175.8
IIA	153.4	164.2	175.5
IIB	157.5	167.8	178.6
IIIA	162.5	173.5	185.0

ΔT_c for T_h equal to

	0°C	25°C	50°C
IA	1.4	1.1	0.9
IIA	1.4	1.1	1.0
IIB	2.5	2.1	1.7
IIIA	1.7	1.4	1.2

Temperatures in Kelvins

Table 8 Cone Temperatures for ϵ_c and ϵ_h Equal to 0.07

	T_c for T_h equal to		
Design	0°C	25°C	50°C
IA	156.2	167.6	179.4
IIA	155.6	167.1	179.0
IIB	158.7	169.8	181.4
IIIA	164.1	175.8	187.9

	ΔT_c for T_h equal to		
	0°C	25°C	50°C
IA	3.6	4.0	4.5
IIA	3.6	4.0	4.5
IIB	3.7	4.1	4.5
IIIA	3.3	3.7	4.1

Temperatures in Kelvins

Table 9 Cone Temperatures for S_i Equal to 80

	T_c for T_h equal to		
Design	0°C	25°C	50°C
IA	156.2	167.8	179.7
IIA	155.7	167.5	179.5
IIA	158.7	170.1	181.9
IIIA	164.6	176.6	188.9

	ΔT_c for T_h equal to		
	0°C	25°C	50°C
IA	3.6	4.2	4.8
IIA	3.7	4.4	5.0
IIB	3.7	4.4	5.0
IIIA	3.8	4.5	5.1

Temperatures in Kelvins

Table 10 Cone Temperatures for Degraded Radiative Properties

Design	$0^{o}C$	$25^{o}C$	$50^{o}C$
IA	160.7	172.5	184.6
IIA	160.4	172.2	184.5
IIB	164.2	175.6	187.5
IIIA	169.1	181.2	193.7

ΔT_c for T_h equal to

	$0^{o}C$	$25^{o}C$	$50^{o}C$
IA	8.1	8.9	9.7
IIA	8.4	9.1	10.0
IIB	9.2	9.9	10.6
IIIA	8.3	9.1	9.9

Temperatures in Kelvins

Table 11 Thermal Inputs to the Cone of Design IIIA

	Nominal		Maximum	
Source	T_c = 172.1K		T_c = 181.2K	
	$W \cdot cm^{-2}$	%	$W \cdot cm^{-2}$	%
H_e	4.02×10^{-4}	8.1	6.42×10^{-4}	10.5
H_h	11.31×10^{-4}	22.7	15.78×10^{-4}	25.8
H_i	24.43×10^{-4}	49.1	29.67×10^{-4}	48.5
H_k	10.00×10^{-4}	20.1	9.28×10^{-4}	15.2

$T_h = 25^{\circ}C$

4.0 PATCH TEMPERATURE RANGES

The steady-state thermal balance equation of either patch may be written as:

$$\sigma A_p T_p^4 = \Phi_k + \Phi_r + \Phi_o + \Phi_j + \Phi_i, \tag{13}$$

where A_p = black radiating area of patch

Φ_k = conductive input through supports, leads, and anti-frost enclosure

Φ_r = radiative input from cone walls

Φ_o = radiative input through optical opening

Φ_j = joule input from detector bias

Φ_i = radiative (equivalent) input through multilayer insulation

For the first (120K InAs) patch, the conductive input is given by

$$\Phi_k = K_{p1} (T_c - T_{p1}) \tag{14}$$

where K_{p1} is the thermal conductance between the cone and patch and T_{p1} the patch temperature. For the second (90K HgCdTe) patch, the conductive input is given by

$$\Phi_k = K_1 (T_{p1} - T_{p2}) + K_2 (T_c - T_{p2}) \tag{15}$$

where K_1 is the thermal conductance between patches, K_2 the thermal conductance between the cone and second patch, and T_{p2} the temperature of the second patch.

The radiative input from the low-emissivity cone walls above the black patch area is given by

$$\Phi_r = A_p \quad \epsilon_{pc} \quad \sigma T_c^4 \tag{16}$$

where ϵ_{pc} is the effective patch-to-cone emissivity. The values of ϵ_{pc} for the three cone designs and for two values of effective specular cone wall emissivity are given in Section 5.0.

The radiative input through the optical connection to a patch is estimated in Appendix II. The result is $\Phi_o = 1 \times 10^{-3}$ W. The InAs detectors in the first patch are photovoltaic, so that the joule input Φ_j is zero. The HgCdTe detectors in the second patch have typical optimum bias powers in the range from 0.5×10^{-3} to 1×10^{-3} W. The resultant joule heat for 4 detectors then range from 2×10^{-3} to 4×10^{-3} W.

The multilayer insulation between the patch (back and side areas) and cone structure has a nominal shielding factor of 200. The areas covered are listed in Table 12 together with the black patch areas A_p. The smaller detector package required for the second patch allows a reduction in the insulated area (See Section 6.0). A modification in which the area of patch 1 was decreased and that of patch 2 increased was also studied. The corresponding insulation and black areas are listed in Table 13. The patch areas allow for patch-cone and patch-patch clearances of 0.050 inch.

Table 12 Patch Surface Areas

Design	A_p	A_{ip} Patch 1	Patch 2
IA	6.404	8.894	7.715
IIA	8.615	11.85	10.12
IIB	10.173	14.41	12.26
IIIA	6.404	8.894	7.715

All in square inches.

Table 13 Modified Patch Areas

	Patch 1		Patch 2	
Design	A_p	A_{ip}	A_p	A_{ip}
IA	4.192	5.939	8.523	9.912
IIA	5.697	7.950	11.441	13.02
IIB	6.782	9.872	13.493	15.70
IIIA	4.192	5.939	8.523	9.912

All in square inches.

4.1 First Patch

The connections between the cone and the first patch are given in Table 14. Note that all the electrical leads to the second patch run through, and are thermally grounded at, the first patch. All connections contribute a thermal conductance of $K_{p1} = 1.786 \times 10^{-4}$ W · K^{-1}.

Table 14 Connections Between Cone and First Patch

No.	To	Dia. (Inch)	Material
15	InAs Array	3.3×10^{-3}	chromel
5	HgCdTe Array	2.0×10^{-3}	nickel
4	patch temp. meas.	3.3×10^{-3}	chromel
4	patch heaters	3.3×10^{-3}	chromel
4	supports	1/8 x 3/32	synthane
1	enclosure	0.775 (av.)	1×10^{-3} inch polyimide

All are 1.6 inches long.

The patch temperatures of the four selected designs were first calculated for the following set of nominal radiative properties and parameters.

α_c = solar absorptivity of cone wall = 0.13

ϵ_c = infrared absorptivity (and emissivity) of cone wall = 0.05

ϵ_h = infrared emissivity of shield = 0.05

ϵ_d = infrared emissivity of cone end = 1

s_i (c) = shielding factor of cone insulation = 100

s_i (p) = shielding factor of patch insulation = 200

K_{p1} = cone-patch thermal conductance = 1.786×10^{-4} W · K^{-1}

$\Phi_o + \Phi_j$ = detector thermal inputs = 1×10^{-3} W

The nominal areas are these listed in Table 12. The first, third, fourth, and fifth properties are needed to establish the cone temperature upon which the patch temperature depends.

The resultant patch temperatures are listed in Table 15 for three values of housing temperature T_h together with the patch temperature differences from those of design IIB. Increasing the cooler size from a nominal 12 inches to 14 inches (Tables 1 and 2, Section 2.0) has a significant influence on the patch temperature (designs IA and IIA). Reducing the shield and cone end size produces smaller temperature increases (designs IA and IIIA). On the other hand, maximizing the patch area within a given nominal size has little influence on performance (designs IIA and IIB). A variation in housing temperature of ± 25 degrees C about 25 degrees C changes the patch temperature by approximately ± 3.7K.

Table 15 Patch 1 Temperatures for Nominal Radiative Properties

	T_{p1} for T_h equal to		
Design	0°C	25°C	50°C
IA	91.4	95.0	98.7
IIA	87.2	90.8	94.5
IIB	86.8	90.4	94.2
IIIA	94.1	97.8	101.7
	ΔT_{p1} for T_h equal to		
	0°C	25°C	50°C
IA	4.6	4.6	4.5
IIA	0.4	0.4	0.3
IIB	0	0	0
IIIA	7.3	7.4	7.5

Temperatures in Kelvins.

Next, the thermal properties were degraded from the nominal values in order to study their influence on the patch temperature. The solar absorptivity of the cone wall α_c, infrared emissivity of the cone wall ϵ_c and emissivity of the shield ϵ_h, and insulation shielding factors s_i (c) and s_i (p), were degraded individually and simultaneously. The degradation factors were the same as those used in the study of the behavior of the cone (Section 3.0). The results are given in Tables 16 to 19, which show both the patch temperatures and their increases from the nominal values.

The lowest patch temperatures are attained in all cases by design IIA and IIB, which differ little in performance. However, because design IIB displays the greatest sensitivity to changes in thermal properties among all designs (true also of the cone, Section 3.0), one would probably select IIA. Otherwise, there is a direct trade-off between patch temperature and physical size. A reduction from the nominal 14-inch size to the 12-inch size (design IIA) increases the patch temperature by an average of 4.2K. A further reduction in the shield length from 14.583 inches (IIA) to 12 inches (IIIA) increases the patch temperature by an additional 2.9 K.

Table 16 Patch 1 Temperatures for α_c Equal to 0.22

T_{p1} and ΔT_{p1} for T_h equal to

Design	0°C	25°C	50°C
IA	91.9, 0.5	95.4, 0.4	99.0, 0.3
IIA	87.6, 0.4	91.1, 0.3	94.8, 0.3
IIB	87.7, 0.9	91.1, 0.7	94.8, 0.6
IIIA	94.7, 0.6	98.3, 0.5	102.1, 0.4

Temperatures in Kelvins

Table 17 Patch 1 Temperatures for ϵ_c and ϵ_h equal to 0.07

T_{p1} and ΔT_{p1} for T_h equal to

Design	0°C	25°C	50°C
IA	94.3, 2.9	98.4, 3.4	102.6, 3.9
IIA	90.2, 3.0	94.3, 3.5	98.6, 4.1
IIB	90.4, 3.6	94.5, 4.1	98.9, 4.7
IIIA	97.1, 3.0	101.3, 3.5	105.7, 4.0

Temperatures in Kelvins

Table 18 Patch 1 Temperatures for s_i Reduced by 0.8X

Design	T_{p1} and ΔT_{p1} for T_h equal to 0°C	25°C	50°C
IA	92.8, 1.4	96.7, 1.7	100.7, 2.0
IIA	88.65, 1.45	92.5, 1.7	96.5, 2.0
IIB	88.4, 1.6	92.3, 1.9	96.4, 2.2
IIIA	95.6, 1.5	99.6, 1.8	103.7, 2.0

Temperatures in Kelvins.

Table 19 Patch 1 Temperatures for Degraded Radiative Properties

Design	T_{p1} and ΔT_{p1} for T_h equal to 0°C	25°C	50°C
IA	96.1, 4.7	100.4, 5.4	104.8, 6.1
IIA	92.2, 5.0	96.45, 5.65	101.0, 6.5
IIB	92.7, 5.9	97.05, 6.65	101.65, 7.45
IIIA	99.2, 5.1	103.6, 5.8	108.2, 6.5

Temperatures in Kelvins.

To interconnect an instrument with 14-element array, the size of the optical port between the cone and the patch may have to be enlarged. Increasing the size of the optical connection increases both the conductive coupling (through the enclosure) to the cone and the radiative input from the opening. Table 20 lists the patch temperatures for an additional optical opening and enclosure (See Table 14 and Appendix B).

Table 20 Patch 1 Temperatures For Two Optical Ports

	T_{p1} and ΔT_{p1} for T_h equal to		
Design	0°C	25°C	50°C
IA	92.9, 1.5	96.4, 1.4	100.1, 1.4
IIA	88.5, 1.3	92.0, 1.2	95.6, 1.1
IIB	88.0, 1.2	91.5, 1.1	95.25, 1.05
IIIA	95.5, 1.4	99.2, 1.4	102.9, 1.2

Temperatures in Kelvins, nominal radiative properties.

Because all the designs had patch temperatures well below the nominal requirement of 120K, the effect of a reduction in patch radiating area was also studied (Table 13). The resultant patch temperatures are shown in Table 21 for the nominal radiative properties and in Table 22 for the degraded radiative properties. The temperature increases shown are relative to the corresponding nominal area temperatures (Tables 15 and 19, respectively).

Table 21 Patch 1 Temperatures for Reduced Area and Nominal Radiative Properties

	T_{p1} and ΔT_{p1} for T_h equal to		
Design	0°C	25°C	50°C
IA	97.5, 6.1	101.3, 6.3	105.1, 6.4
IIA	92.8, 5.6	96.5, 5.7	100.3, 5.8
IIB	92.0, 5.2	95.7, 5.3	99.5, 5.3
IIIA	100.35, 6.25	104.2, 6.4	108.1, 6.4

Temperatures in Kelvins.

Table 22 Patch 1 Temperatures for Reduced Area and Degraded Radiative Properties

Design	T_{p1} and ΔT_p for T_h equal to 0°C	25°C	50°C
IA	102.0. 5.9	106.4, 6.0	110.8, 6.0
IIA	97.55, 5.35	101.8, 5.35	106.3, 5.3
IIB	97.55, 4.85	101.9, 4.85	106.4, 4.75
IIIA	105.1, 5.9	109.6, 6.0	114.2, 6.0

Temperatures in Kelvins.

One may define the sensitivity of a patch to changes in a given parameter as the ratio of the temperature change to the factor by which the parameter has been degraded. The sensitivities of patch 1 to the parameters studied are given in Table 23, where the temperature change is the average over all designs and housing temperatures.

Table 23 Sensitivity of Patch 1 to Design Parameters

Parameter	Degradation Factor	Temperature Increase (K)	Sensitivity (K)
Solar absorptivity	1.69	0.49	0.29
Infrared emissivity	1.40	3.64	2.60
Reciprocal insulation factor	1.25	1.77	1.42
Optical connection	2	1.27	0.64
Reciprocal radiating area	1.53	5.90	3.86

The design is most sensitive to a reduction in the patch area. This not only reduces the power emitted at a given temperature but also increases the cone-patch radiative coupling (Section 5.0). For a given patch area, the infrared emissivity of the low-emissivity surfaces is the most critical parameter.

4.2 Second Patch

The connections between the first patch and second patch and between the cone and second patch are given in Table 24. The respective thermal conductances are $K_1 = 1.1035 \times 10^{-4}$ W · K^{-1} and $K_2 = 4.0 \times 10^{-6}$ W · K^{-1}.

Table 24 Connections to Second Patch

No.	to	dia. (inch)	material
5	HgCdTe Array	2×10^{-3}	nickel
2	patch temp. meas.	3.3×10^{-3}	chromel
2	patch heater	3.3×10^{-3}	chromel
2	supports	1/8 x 3/32	synthane
1	enclosure*	0.775 (av.)	1×10^{-3} inch polyimide

* Connected to cone, all others are connected to the first patch.

All are 1.2 inches long, except the enclosure, which is 2.4 inches.

The patch temperatures of the four selected designs were first calculated for the same nominal radiative properties as listed in Section 4.1, except that the thermal conductance had the values given above and $\Phi_o + \Phi_j$ was equal to 3×10^{-3} W. The four detectors on the second patch require a bias, which was set at a nominal value of 0.5×10^{-3} W per detector. The nominal patch areas are listed in Table 12.

The resultant patch temperatures are listed in Table 25 for three values of housing temperature T_h together with the differences from design IIB. It is assumed that the first patch is maintained at a temperature of 120K. Again, there is little difference in performance between designs IIA and IIB. Also, the trade-off between physical size and patch temperature is still evident, although the differences among the designs has been reduced. A housing temperature variation of ± 25 degrees C about 25 degrees C produces average patch temperature variations of +2.2 K and -1.8 K.

Table 25 Patch 2 Temperatures for Nominal Radiative Properties

	T_{p2} and ΔT_{p2} for T_h equal to		
Design	0°C	25°C	50°C
IA	81.3, 3.1	82.7, 2.3	84.95, 1.45
IIA	78.8, 0.6	80.7, 0.3	83.0, 0
IIB	78.2, 0	80.4, 0	83.0, 0
IIIA	82.3, 4.1	84.0, 3.6	86.0, 3.0

Temperatures in Kelvins; T_{p1} = 120 K.

Next, the thermal properties were degraded from the nominal values in the manner described in Section 4.1. The resultant patch temperatures are listed in Tables 26 to 29. The listed changes in patch temperatures are the increases above the nominal values. The increases in T_{p2} are consistently less than the increases in T_{p1} for the same degradation. This is a consequence of the reduced thermal coupling to the cone. Design IIB again displays the greatest sensitivity to changes in the thermal properties.

Table 26 Patch 2 Temperatures for α_c Equal to 0.22

	T_{p2} and ΔT_{p2} for T_h equal to		
Design	0°C	25°C	50°C
IA	81.45, 0.15	82.9, 0.2	84.6, 0.15
IIA	79.0, 0.2	80.9, 0.2	83.2, 0.2
IIB	78.7, 0.5	80.9, 0.5	83.4, 0.4
IIIA	82.6, 0.2	84.2, 0.2	86.2, 0.2

Temperatures in Kelvins; T_{p1} = 120 K.

Table 27 Patch 2 Temperatures for ϵ_c and ϵ_h Equal to 0.07

	T_{p2} and ΔT_{p2} for T_h equal to		
Design	0°C	25°C	50°C
IA	83.5, 2.2	85.6, 2.9	88.0, 3.55
IIA	81.25, 2.45	83.8, 3.1	86.8, 3.8
IIB	81.3, 3.1	84.2, 3.8	87.5, 4.5
IIIA	84.9, 2.6	87.2, 3.2	89.9, 3.9

Temperatures in Kelvins; T_{p1} = 120 K.

Table 28 Patch 2 Temperatures for s_i Reduced by 0.8X

	T_{p2} and ΔT_{p2} for T_h equal to		
Design	0°C	25°C	50°C
IA	82.0, 0.7	83.7, 1.0	85.75, 1.3
IIA	79.7, 0.9	82.0, 1.3	84.6, 1.6
IIB	79.3, 1.1	81.9, 1.5	84.85, 1.85
IIIA	83.2, 0.9	85.2, 1.2	87.5, 1.5

Temperatures in Kelvins; T_{p1} = 120 K.

Table 29 Patch 2 Temperatures for Degraded Radiative Properties

	T_{p2} and ΔT_{p2} for T_h equal to		
Design	0°C	25°C	50°C
IA	84.7, 3.4	87.0, 4.3	89.7, 5.25
IIA	82.6, 3.8	85.45, 4.75	88.75, 5.75
IIB	83.1, 4.9	86.3, 5.9	89.9, 6.9
IIIA	86.25, 3.95	88.9, 4.9	91.9, 5.9

Temperatures in Kelvins; T_{p1} = 120 K.

It may be desirable to increase the detector bias power to improve detector performance. Table 30 shows the patch temperatures for a bias heat of 1×10^{-3} W per element, an increase of 0.5×10^{-3} W. The larger temperature increases are associated with the smaller patch areas.

Table 30 Patch 2 Temperatures for $\Phi_o + \Phi_j$ Equal to 5×10^{-3} W

	T_{p2} and ΔT_{p2} for T_h equal to		
Design	0°C	25°C	50°C
IA	84.4, 3.1	85.7, 3.0	87.3, 2.85
IIA	81.4, 2.6	83.2, 2.5	85.3, 2.3
IIB	80.5, 2.3	82.6, 2.2	85.0, 2.0
IIIA	85.3, 3.0	86.85, 2.85	88.7, 2.7

Temperatures in Kelvins; $T_{p1} = 120$ K

The changes produced by an increase in conductive coupling between patches are given in Table 31. The increase in thermal conductance equals that of an additional patch support. The smaller patch area in designs IA and IIA again results in a greater temperature increase.

Table 31 Patch 2 Temperatures for Three Supports

	T_{p2} and ΔT_{p2} for T_h equal to		
Design	0°C	25°C	50°C
IA	83.4, 2.1	84.7, 2.0	86.3, 1.85
IIA	80.7, 1.9	82.45, 1.75	84.5, 1.5
IIB	80.0, 1.8	82.0, 1.6	84.4, 1.4
IIIA	84.4, 2.1	85.85, 1.85	87.6, 1.6

Temperatures in Kelvins; $T_{p1} = 120$ K

The sensitivities of patch 2 to changes in the thermal parameters are listed in Table 32. The design is most sensitive to an increase in the infrared emissivity of the low-emissivity surfaces, followed by the detector thermal input ($\Phi_o + \Phi_j$) and the conductive coupling.

Table 32 Sensitivity of Patch 2 to Thermal Parameters

Parameter	Degradation Factor	Temperature Increase (K)	Sensitivity (K)
Solar absorptivity	1.69	0.27	0.16
Infrared emissivity	1.40	3.26	2.33
Reciprocal insulation factor	1.25	1.24	0.99
Detector thermal input	1.67	2.62	1.57
Conductive coupling	1.33	1.79	1.35

An attempt was made to improve the performance of the lower temperature patch by increasing its radiating area (Table 13). This was accomplished by transferring the central portion of patch 1 to patch 2. The larger area should also reduce the sensitivity to increases in joule heat and thermal conductance. The resultant patch temperatures are shown in Tables 33 and 34 for the nominal and degraded radiative properties, respectively. The temperature reductions are small for the nominal properties, especially in the case of designs IA and IIIA, and for the degraded properties, there is actually an increase in patch temperature under some conditions.

The increase in radiating area is apparently offset by the increased radiative coupling to the cone. Although the increase in area was obtained by means of elements from the central portion of the first patch, the patch-to-cone emissivity was still increased. This is especially true of the cone design employed in IA and IIIA (see Section 5.0). If the performance of these designs is to be improved by an increase in patch area, the increase must be obtained by enlarging the dimensions of the entire cooler, i.e., increasing the nominal size to more than 12 inches.

Table 33 Patch 2 Temperatures for Increased Area and Nominal Radiative Properties

	T_{p2} and ΔT_{p2} for T_h equal to		
Design	0°C	25°C	50°C
IA	79.5, -1.8	81.6, -1.1	84.0, -0.45
IIA	76.1, -2.7	78.3, -2.4	80.9, -2.1
IIB	76.0, -2.2	78.5, -1.9	81.45, -1.55
IIIA	81.0, -1.3	83.3, -0.7	86.05, -0.05

Temperatures in Kelvins; T_{p1} = 120 K

Table 34 Patch 2 Temperatures for Increased Area and Degraded Radiative Properties

	T_{p2} and ΔT_{p2} for T_h equal to		
Design	0°C	25°C	50°C
IA	83.6, -1.1	86.6, -0.4	90.05, +0.35
IIA	80.6, -2.0	83.8, -1.65	87.45, -1.3
IIB	81.6, -1.5	85.1, -1.2	89.1, -0.8
IIIA	85.7, -0.55	89.05, +0.15	92.8, +0.9

Temperatures in Kelvins; T_{p1} = 120 K

The thermal inputs to the second patch of design IIIA are listed in Table 35 for the nominal (Table 25) and degraded (Table 29) radiative thermal properties. The housing temperature is 25 degrees C in both cases. It is seen that the input through the multilayer insulation is small and that the remaining input is roughly equally divided among the other three sources.

Table 35 Thermal Inputs to Patch 2 of Design IIIA

	Nominal T_c = 172.1 K		Degraded T_c = 181.2 K	
Source	mW	%	mW	%
Φ_k	4.33	37.2	3.80	26.0
Φ_r	3.16	27.1	6.01	41.2
$\Phi_o + \Phi_j$	3.00	25.7	3.00	20.5
Φ_i	1.17	10.0	1.79	12.3

$T_h = 25^oC$

5.0 RADIATIVE COUPLING FACTORS

In order to determine the radiative interchange between two radiant cooler areas and between a cooler area and an external area, it is necessary to know one or several view factors (The fraction of power diffusely emitted from one area that directly strikes a second area is the view factor from the first area to the second).

The view factors required for thermal analysis of the radiant cooler are:

(a) $F_{p-m}(n)$ = view factor from the patch to the cone mouth images seen by n specular reflections in the cone walls.

(b) $F_{d-h(n)}$ = view factor from the cone end to the shield mouth images seen by n specular reflections in the shield wall.

(c) F_{d-e} = view factor from the cone end to the visible region of the earth.

(d) $F_{m-e(n)}$ = view factor from the cone mouth to the visible region of the earth whose radiation is reflected n times in the cone walls.

The view factors were evaluated by means of the specular image array and contour integral techniques described in the final report on Contract NAS5-11683 (Part I, 8 April - 31 October 1969) and in Applied Optics for January 1970 (p. 185).

The view factors (a) are used to determine the patch-cone radiative coupling factor or effective patch-to-cone emissivity. (Final Report on Contract NAS5-10113, December 1967, Section 1.3).

$$\epsilon_{pc} = 1 - \Sigma_n \; F_{p-m}(n) \; (1 - \epsilon_c)^n, \tag{17}$$

where ϵ_c is the emissivity of the cone walls and the patch is black (emissivity of one).

The view factors (b) are used to determine the effective emissivity of the shield as seen from the cone end (equal to the effective absorptivity of the shield for cone end radiation),

$$A_{dh} = \Sigma_n \; a_n \; F_{d-h}(n), \tag{18}$$

where a_n is the emissivity (absorptivity) produced by n shield wall reflections. For infrared radiation, $a_n = 1 - (1 - \epsilon_h)^n$, where ϵ_h is the infrared absorptivity (emissivity) of the shield walls. Using the conservation condition

$$\Sigma F_{d-h\,(n)} = 1, \tag{19}$$

the above may also be written as

$$A_{dh} = 1 - \Sigma F_{d-h\,(n)} (1 - \epsilon_h)^n, \tag{20}$$

The cone end-shield radiative coupling factor or effective emissivity is obtained by multiplying a_{dh} by the emissivity ϵ_d of the cone end. This is the case because radiation leaving the cone end by emission or reflection never returns when the shield walls are specularly reflecting and outward sloping (a condition which also holds between the patch and cone walls).

The view factors (c) and (d) are used to determine the absorptivity of the cone end and cone mouth, respectively, for radiation from the earth. In the case of the cone mouth, multiple reflections at the cone walls must be taken into account. The effective absorptivity for earth radiation is then

$$a_{me} = \Sigma a_n F_{m-e\,(n)}, \tag{21}$$

where a_n is the absorptivity produced by n cone wall reflections. For infrared, $a_n = 1 - (1-\epsilon_c)^n$ and for reflected sunlight $a_n = 1 - (1- \alpha_c)^n$, where ϵ_c and α_c are the infrared and solar absorptivity, respectively.

The view factors $F_{p-m(o)}$ and $F_{p-m(2)}$ were calculated for 12 equal elemental areas over the patch opening. By symmetry there are 6 different view factors, designated A through F in Figure 2 . Since the elements are equal in size, the view factor for the entire patch is just the average of the elements. No more than two reflections are needed for a patch ray to leave the cone, so that the view factor to the first reflection images of the cone mouth (Figure 2) is given by

$$F_{p-m(1)} = 1 - [F_{p-m(o)} + F_{p-m(2)}] . \tag{22}$$

The results are listed in Table 36 for the three cone designs. The cone of cooler design IIIA is identical to that of design IA.

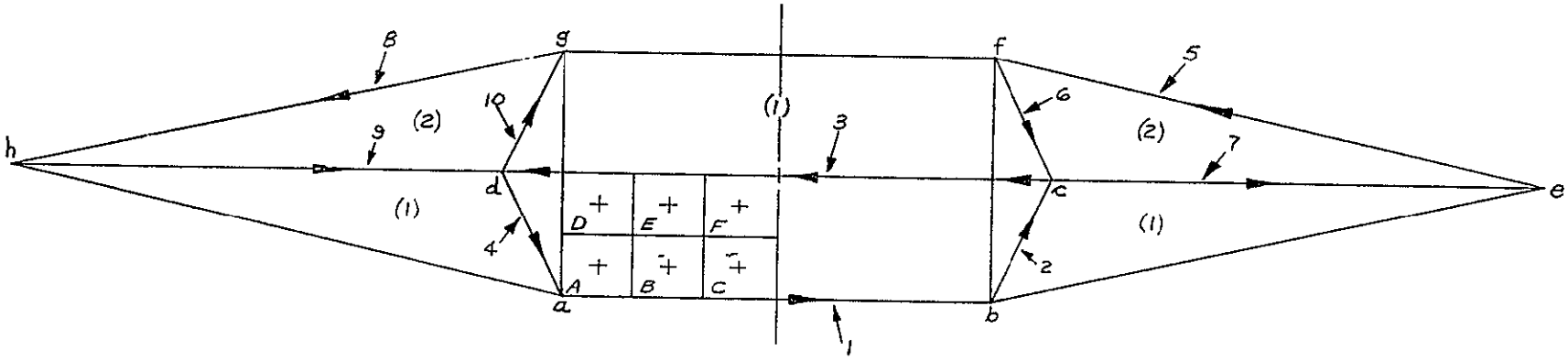

Figure 2 Cone Mouth Reflection Pattern Projected onto Plane of Patch (Design IA)

The patch opening was divided into two equal rectangular areas, one for each of the required patch temperatures. The division line cuts the available width in two. Thus area 2 includes the elements A, B, and C and area 1 elements D, E, and F. The cone-patch radiative coupling factors (ϵ_{pc}) are listed in Table 37 for areas 1 and 2 as well as for the entire patch opening. Results are given for two values of the effective specular cone wall emissivity ϵ_c.

Table 36

View Factors From Patch to Cone Mouth and Its Images

Design and Area		$F_{p-m(o)}$	$F_{p-m(1)}$	$F_{p-m(2)}$
IA (IIIA)	Total	0.56738	0.368185	0.06734
	Area 2	0.64070	0.30229	0.06282
	Area 1	0.49406	0.43408	0.07186
IIA	Total	0.57894	0.36627	0.05479
	Area 2	0.64937	0.29889	0.05174
	Area 1	0.50851	0.43364	0.05785
IIB	Total	0.55037	0.36508	0.08455
	Area 2	0.62724	0.29510	0.07766
	Area 1	0.47350	0.43506	0.09144

Table 37

Patch-Cone Radiative Coupling Factor

	Entire Patch		Area 2		Area 1	
Design	ϵ_{pc} (0.05)	ϵ_{pc} (0.07)	ϵ_{pc} (0.05)	ϵ_{pc} (0.07)	ϵ_{pc} (0.05)	ϵ_{pc} (0.07)
IA (IIIA)	0.0221	0.0320	0.0154	0.0238	0.0287	0.0401
IIA	0.0237	0.0330	0.0200	0.0279	0.0273	0.0382
IIB	0.0265	0.0370	0.0223	0.03115	0.0307	0.0428

(ϵ_c) = effective cone wall specular emissivity

Area 2 with its lower value of cone-patch radiative coupling would, of course, be selected for operation at the lower temperature (90 K) in any design. Also, on the basis of cone-patch coupling, one would select design IA or IIIA. The difference in ϵ_{pc} between area 2 and area 1 and between area 2 and the entire patch is quite pronounced in design IA (IIIA).

If the patch opening were divided into equal areas by cutting the length in two, the coupling factors would be the same for each area and equal to the value for the entire patch.

In order to increase the area of the lower temperature patch, the two F elements were transferred from area 1 to area 2. The resultant view factors and cone-patch radiative coupling factors are given in Table 38.

Table 38

Factors for Modified Patch Areas

Design	$F_{p-m(o)}$	$F_{p-m(1)}$	$F_{p-m(2)}$	$\epsilon_{pc}(0.05)$	$\epsilon_{pc}(0.07)$
IA (IIIA)					
Mod. Area 2	0.61392	0.32953	0.05655	0.0220	0.0307
Mod. Area 1	0.47431	0.43676	0.08893	0.0305	0.0426
IIA					
Mod. Area 2	0.62329	0.33228	0.04443	0.02095	0.0293
Mod. Area 1	0.49023	0.43424	0.07553	0.0291	0.0406
IIB					
Mod. Area 2	0.598385	0.327485	0.07413	0.0236	0.03295
Mod. Area 1	0.45433	0.44027	0.10540	0.0323	0.04505

The view factors $F_{d-h(n)}$ between the cone end and shield were calculated in the same manner as those between the patch and cone. The results are listed in Table 39 for the four different designs. The resultant cone end-shield radiative coupling factors are given in Table 40 for the two values of effective specular wall emissivity. The cone end-shield design of IIB is identical to that of IIA.

Table 39

View Factors From Cone End
to Shield Mouth and Its Images

Design	$F_{d-h(o)}$	$F_{d-h(1)}$	$F_{d-h(2)}$
IA	0.57369	0.36427	0.06204
IIA (IIB)	0.57954	0.36634	0.05412
IIIA	0.56535	0.36025	0.07440

Table 40

Cone End-Shield Radiative Coupling Factor

Design	a_{dh} (0.05)	a_{dh}(0.07)
IA	0.0243	0.0339
IIA (IIB)	0.0236	0.0330
IIIA	0.0253	0.0353

(ϵ_h) = effective shield wall specular emissivity.

The variation in a_{dh} among the cooler designs is not large. The largest value is only about 7 percent higher than the lowest value. As a result, there is little to choose on the basis of cone-end to shield radiative coupling.

The view factors from the cone mouth to the earth, $F_{m-e\ (n)}$, and the resultant effective absorptivity for earth radiation, a_{me}, are measures of the shielding of the cone mouth. The view factors vary considerably over the cone mouth area. The maximum values of $F_{m-e(1)}$ are obtained along the top line of the cone mouth, where the total view of the earth is greatest. However, $F_{m-e(2)}$ is zero along this line because all incident earth rays are reflected out after only one cone wall reflection. All values of $F_{m-e(n)}$ are zero along the bottom line of the cone mouth, which coincides with the start of the cone end area.

The value of $F_{m-e(n)}$ was taken as the average at the six points (1 to r) shown in Figure 3. Points s and t lie along a line that divides the cone mouth into two equal areas. The results are listed in Table 41. Representative cases are illustrated in Figures 4 to 6, which show the boundaries of the shield and cone mouth images projected onto the earth disk.

Table 41

View Factors from Cone Mouth to Earth

Design	$F_{m-e(1)}$	$F_{m-e(2)}$	F_{m-e}
IA	0.06491	0.004795	0.069705
IIA	0.063835	0.00474	0.068575
IIB	0.08490	0.00711	0.09201
IIIA	0.07494	0.004795	0.079735

The solar and infrared absorptivities of the cone mouth for earth radiation are given in Table 42 for two values solar and infrared cone wall absorptivity (α_c and ϵ_c). The results are about the same for designs IA and IIA, but 15 percent higher for IIIA and 35 percent higher for IIB.

Table 42

Absorptivities of Cone Mouth for Earth Radiation

	Reflected Solar		Emitted Infrared	
Design	α_{me} (0.13)	α_{me} (0.22)	ϵ_{me} (0.05)	ϵ_{me} (0.07)
IA	9.60×10^{-3}	1.62×10^{-2}	3.71×10^{-3}	5.19×10^{-3}
IIA	9.45×10^{-3}	1.59×10^{-2}	3.65×10^{-3}	5.11×10^{-3}
IIB	12.8×10^{-3}	2.15×10^{-2}	4.94×10^{-3}	6.90×10^{-3}
IIIA	10.9×10^{-3}	1.84×10^{-2}	4.21×10^{-3}	5.89×10^{-3}

(α_c) = cone wall solar absorptivity

(ϵ_c) = cone wall infrared absorptivity

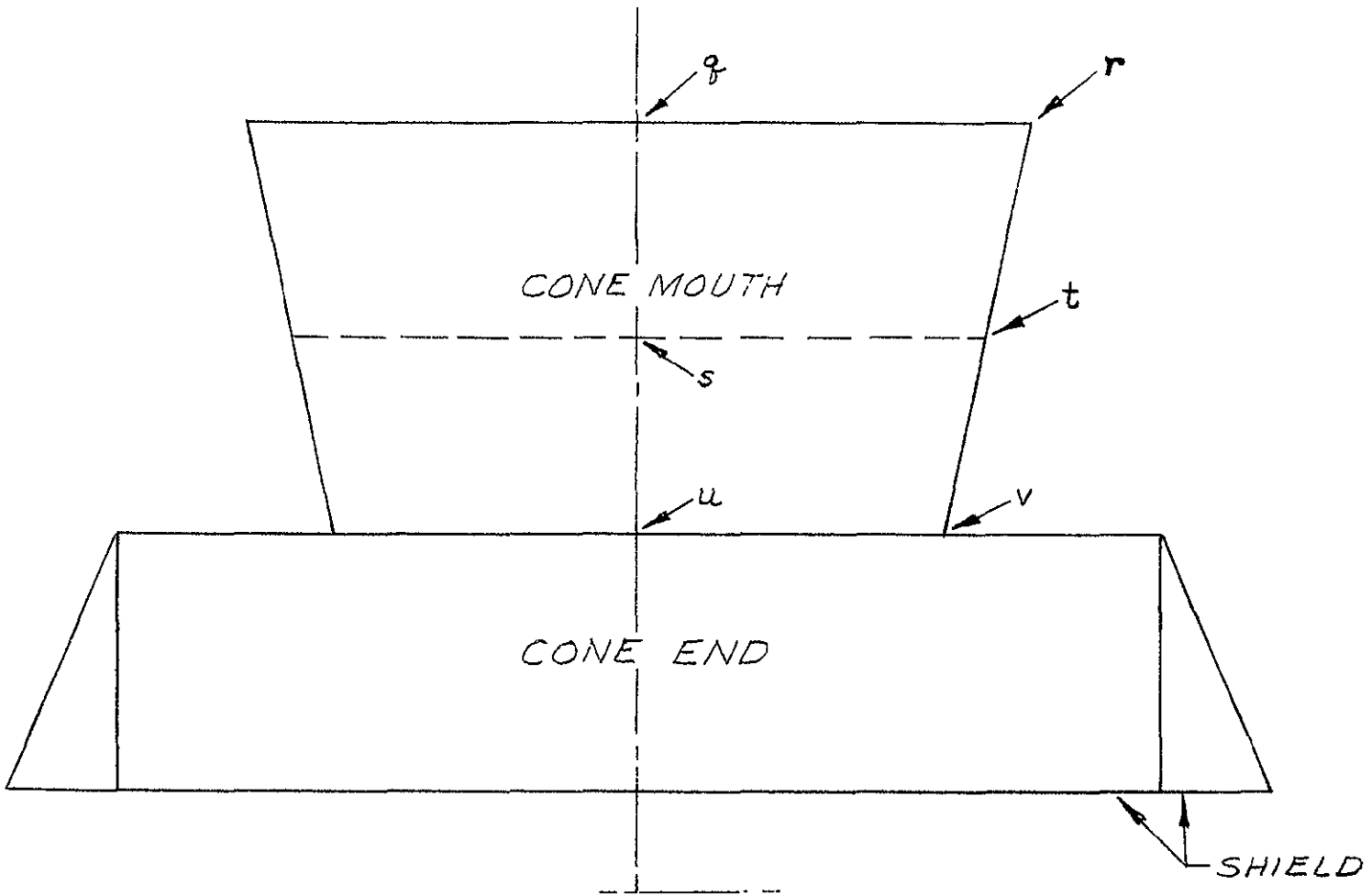

Figure 3 Points on Cone Mouth Used to Determine $F_{m-e(n)}$

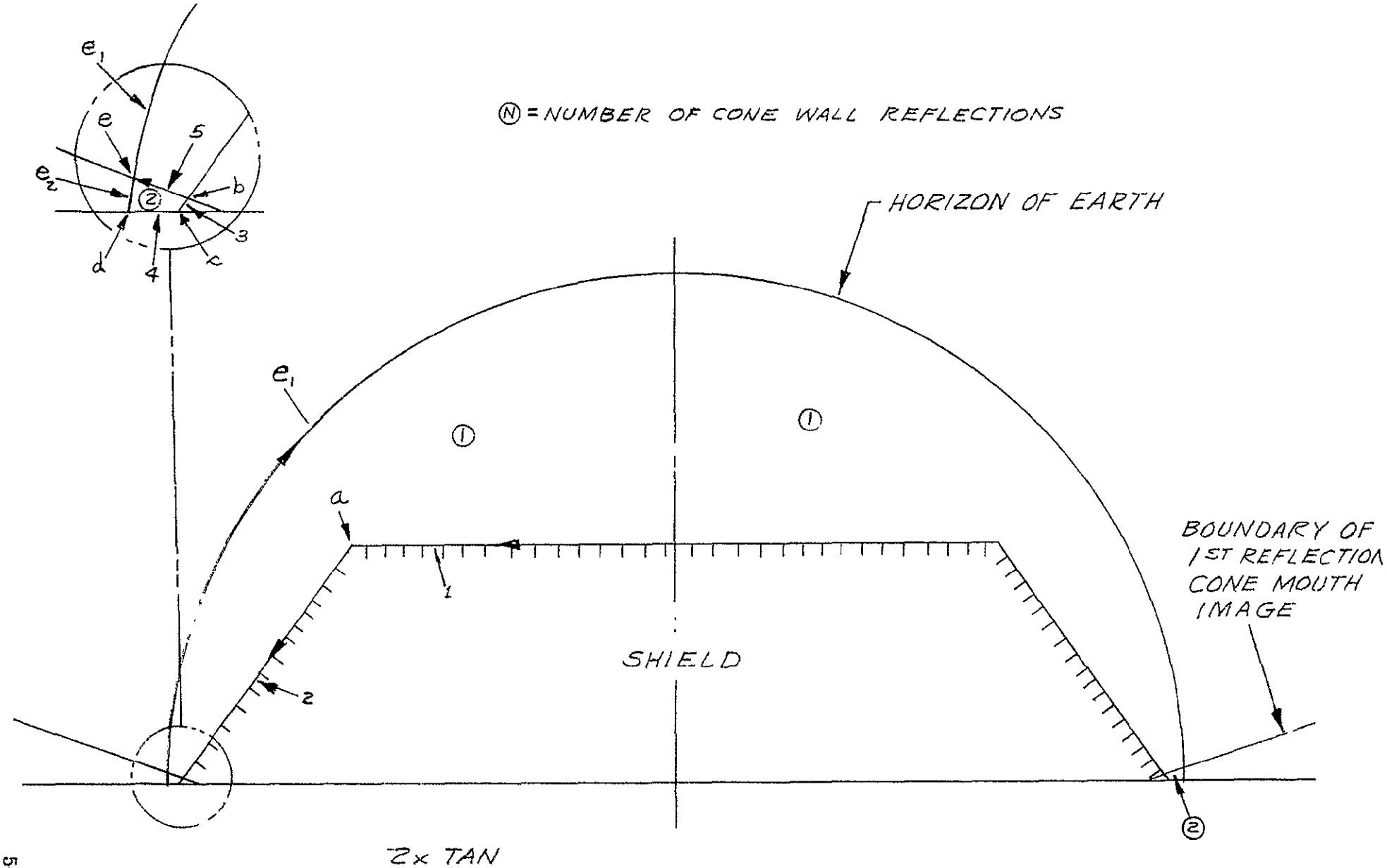

Figure 4 Earth and Shield as Seen From Point s in Design IIB

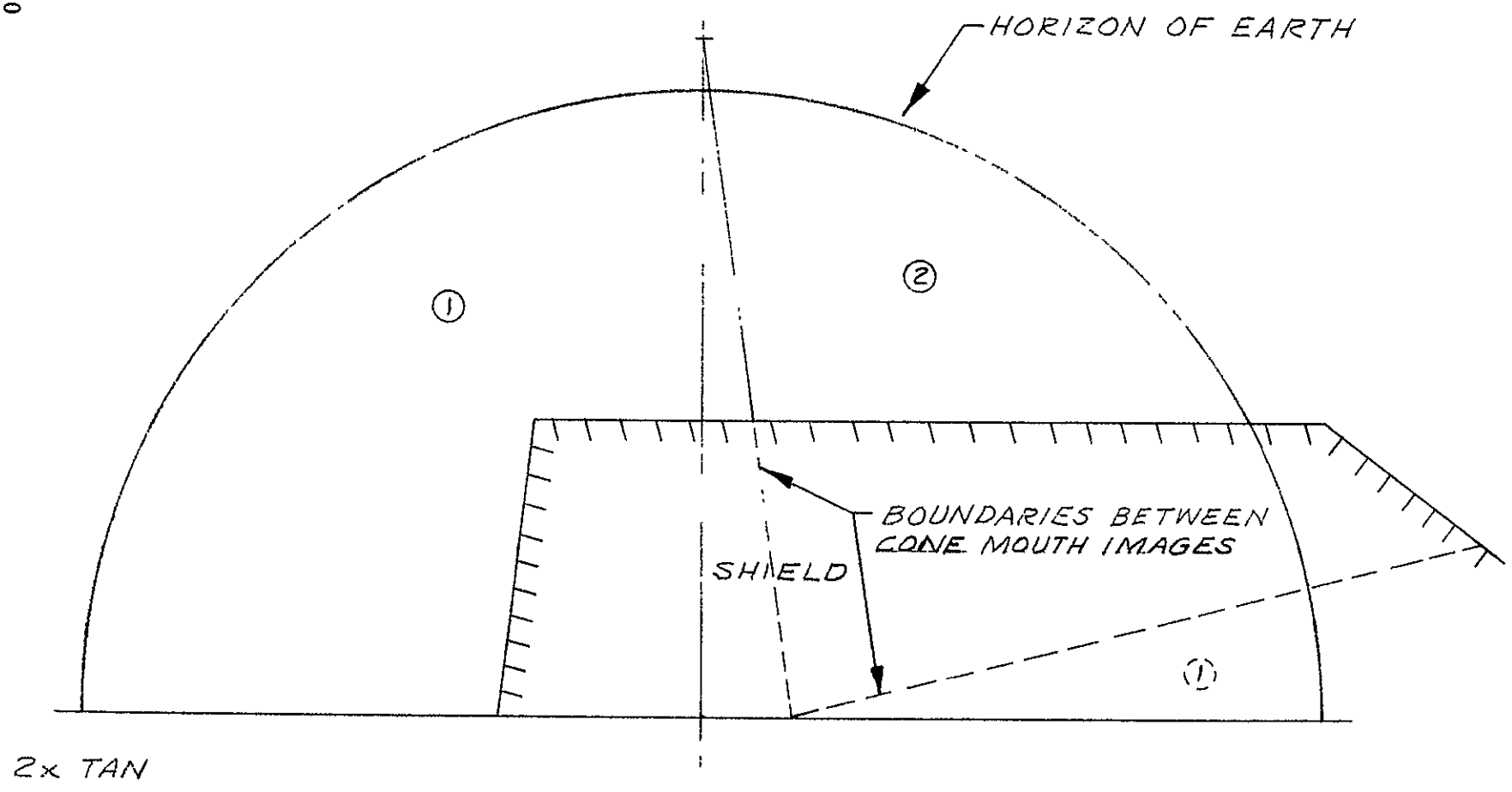

Figure 5 Earth and Shield as Seen From Point t in Design IIB

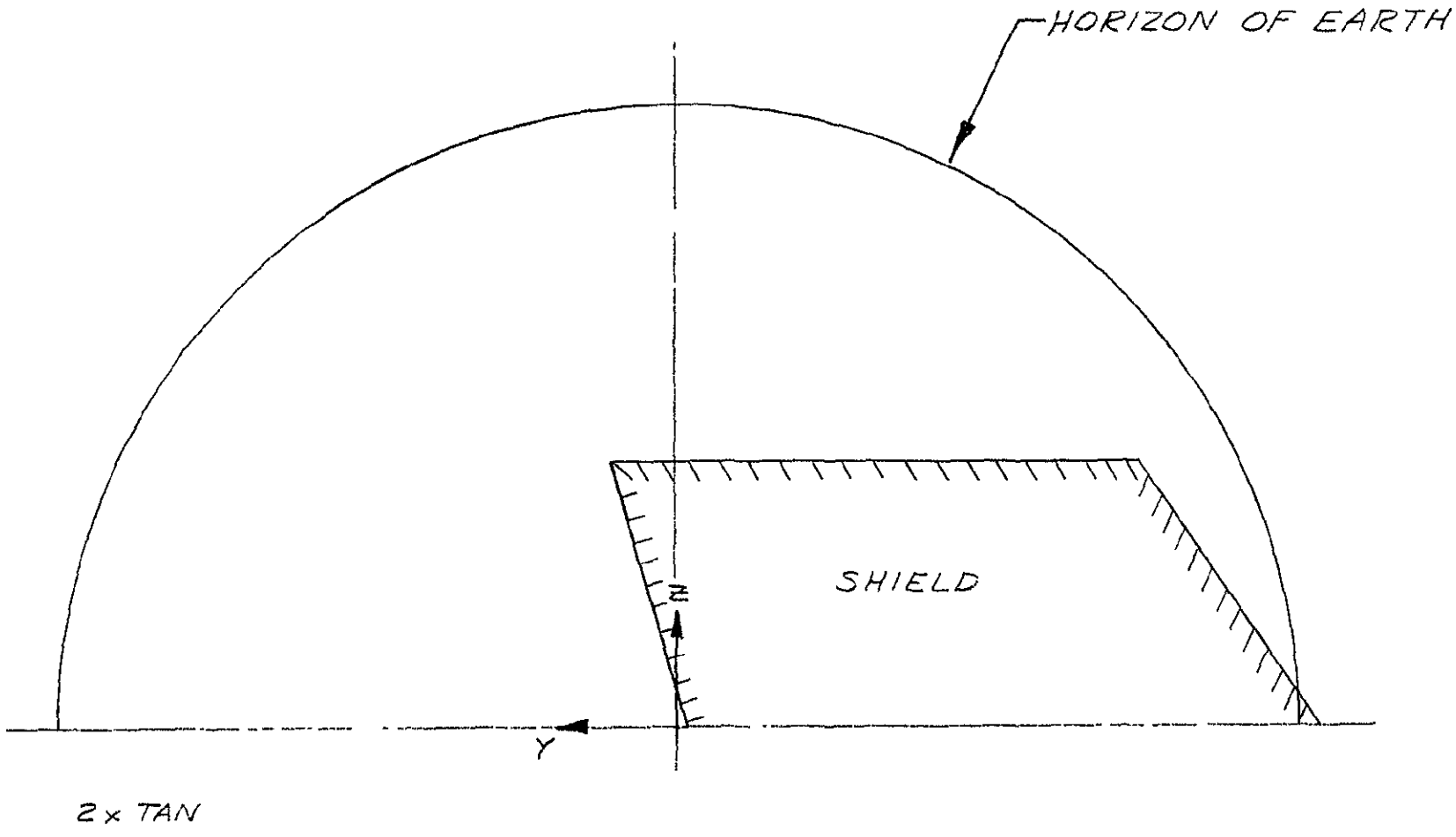

Figure 6 Earth and Shield as Seen From Point r in Design IIIA

6.0 MECHANICAL DESIGN

Figure 7 shows the mechanical layout of a dual patch multi-element radiant cooler. The basic dimensions are those of design IIIA, which has the same cone design as IA. The configuration may change slightly as detailed drawings are completed, but the basic design will remain the same. The front rectangular dimensions of the cooler are 12.0 inches long by 8.5 inches high. The depth is 7.5 inches, which increases to 11.0 inches when the shield-cover is in the down position. The weight of the cooler assembly will be approximately 10 pounds.

The assembly can be divided into two parts, the secondary housing or cone structure that supports the dual patch and the primary housing that supports the secondary housing, shield-cover, and actuator assembly. The cooler parts are mechanically connected by means of low thermal conductivity epoxy-glass (synthane G-10) tubes. Additional thermal insulation is provided by multilayer blankets of aluminzed mylar.

All flat plates will be lightened by means of milled cavities. The size and location of the cavities will be made to achieve natural frequencies above 2000 Hz. Natural frequencies as well as the resulting strains will be checked by experimental methods. Specifically, critical parts will be sinusoidally vibrated at prototype levels.

The low speed, short duty cycle, and light loads involved in actuating the cover permit the use of sleeve bearings and dry film lubricants. Unsealed gear and bearing housing will be used as the dry films present no evaporation problems.

6.1 Construction Details

The housings will be dip brazed assemblies of 6061-T651 aluminum tooling plate with a removable cover to facilitate assembly. The side plates will act as structural members as well as covers. They will have machined-in cavities that leave ribs for stiffeners and vibration control.

The cone will be assembled by means of structural adhesive rather than by dip brazing in order to protect its surface finish. The baseplate and walls of the cone will be machined from 6061-T651 aluminum tooling plate. To obtain high thermal conductance, joints in the assembly will be filled with silver powder loaded epoxy adhesive. The cone assembly will be mounted to the secondary housing by means of screw fasteners in the base plate.

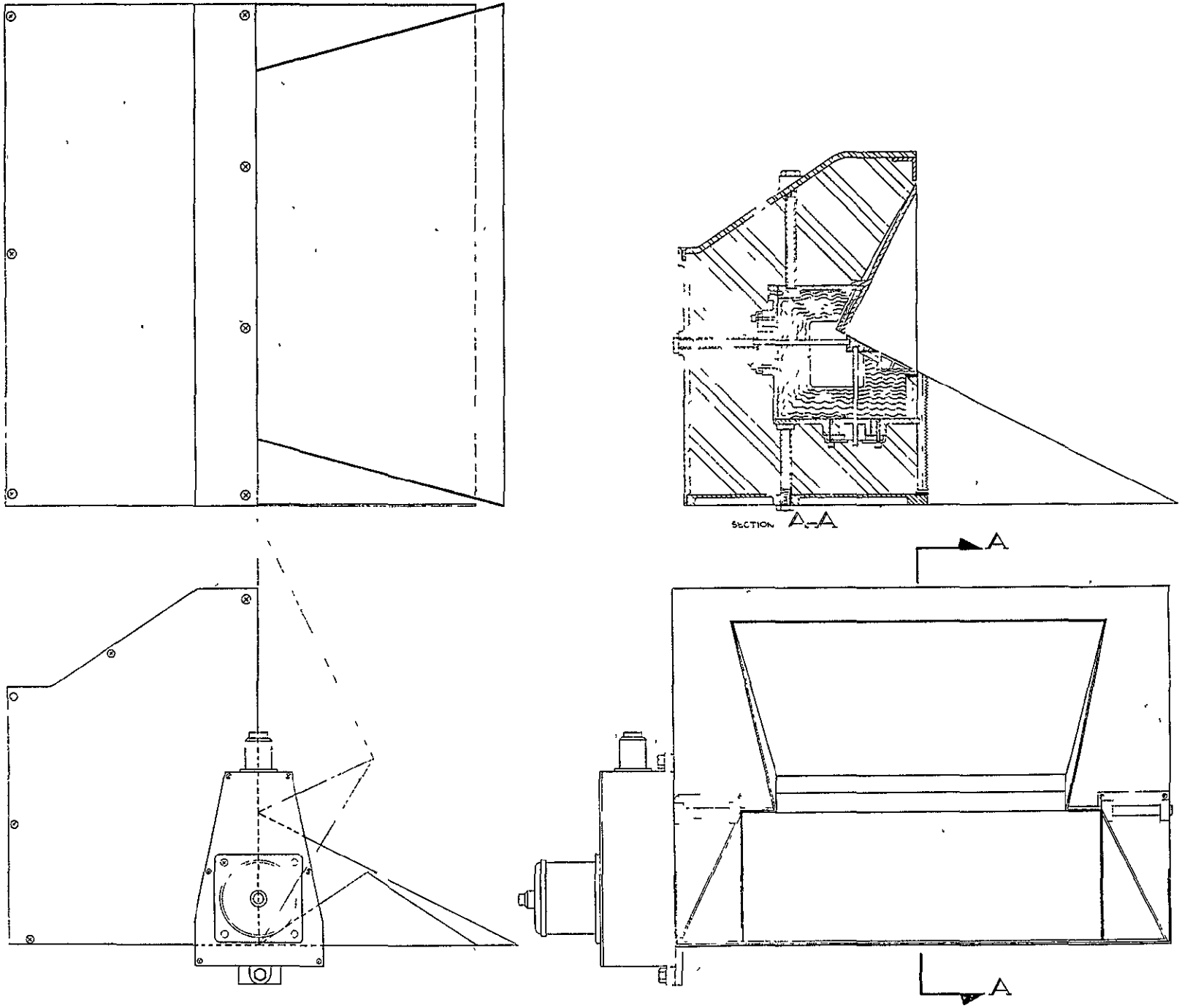

Figure 7. Mechanical Assembly of Dual Patch Multi-Element Radiant Cooler

The dual patch assembly is illustrated by Figures 8 and 9. As shown, it will consist of two separate sub-patches, a 120 K patch and a 90 K patch. The 90 K patch will be supported from the 120 K patch through two synthane tubes. The 120 K patch, in turn, will be supported from the secondary housing by four of these tubes. The support tubes will be 1/8 inch OD by 3/32 inch ID and will be fastened to the patches with adiprene adhesive. Fastening to the housing will be made with taper lock joints to allow the patch assembly to be adjusted in two planes. After the adjustments have been made, the patch assembly will be locked in place with servo clamps.

The patches will be machined from 6061-T651 aluminum tooling plate with the under side polished and gold coated. The exposed (radiating) surface will be coated with 3 M velvet coating 101-C10 black.

The cone shield will also serve as a cone cover to protect the cone during storage as well as to block the cold space look to delay cooler operation or to increase the cooler temperature for defrosting purposes. The shield alone does not cover the cone structure completely, so an auxiliary cover will be mounted below the shield to cover the bottom portion. The shield and cover will be machined from 6061-T651 aluminum tooling plate and be mounted to the primary housing by hinges. The hinges will consist of 1/8 inch diameter stainless steel pins and sleeve bearings of Rulon-A (an aromatic polyimide) filled with glass or ceramic. A film of MoS2 will be applied to both the pins and bearings.

6.2 Cone Cover Actuator

The actuator for the cone cover and shield is shown in Figure 10. The gear train is powered by a unidirectional stepping motor with 20 degree step increments and rotating at two steps per second. The gear ratio between the driver gear and the shield gear is 1.5 to 1.0 and between the driver and the cover gear, 1.5 to 2.0. The shield must rotate 120 degrees and the cover 60 degrees to completely close off the cone mouth and cone end. From the above ratios, the driver gear must then rotate 80 degrees. At two steps, or 20 degrees, per second the least time to cover the cone mouth is 4 seconds. As the gear train rotates the cover and shield to the closed position, a torsion spring is wound up applying torque in the opposite direction. The gear train is prevented from counter rotating by means of a ratchet and pawl, thereby maintaining the covers in the closed position. The motor is de-energized by means of a limit switch when the sector gear reaches the stop. A slip clutch mounted to the driver gear prevents motor damage if the gear train reaches the mechanical stop before the motor shuts off. A solenoid mounted to the gear housing is used for releasing the ratchet, which lets the stored energy in the spring return the cover and shield to the open position.

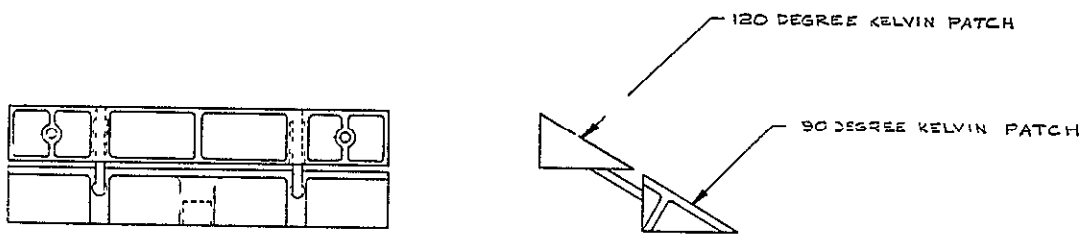

Figure 8 Dual Patch Assembly

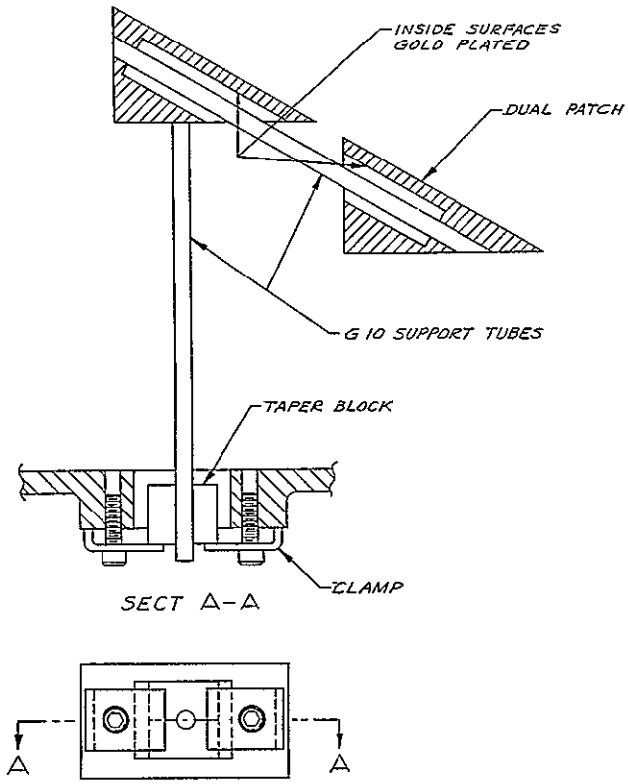

Figure 9 Dual Patch Suspension Detail

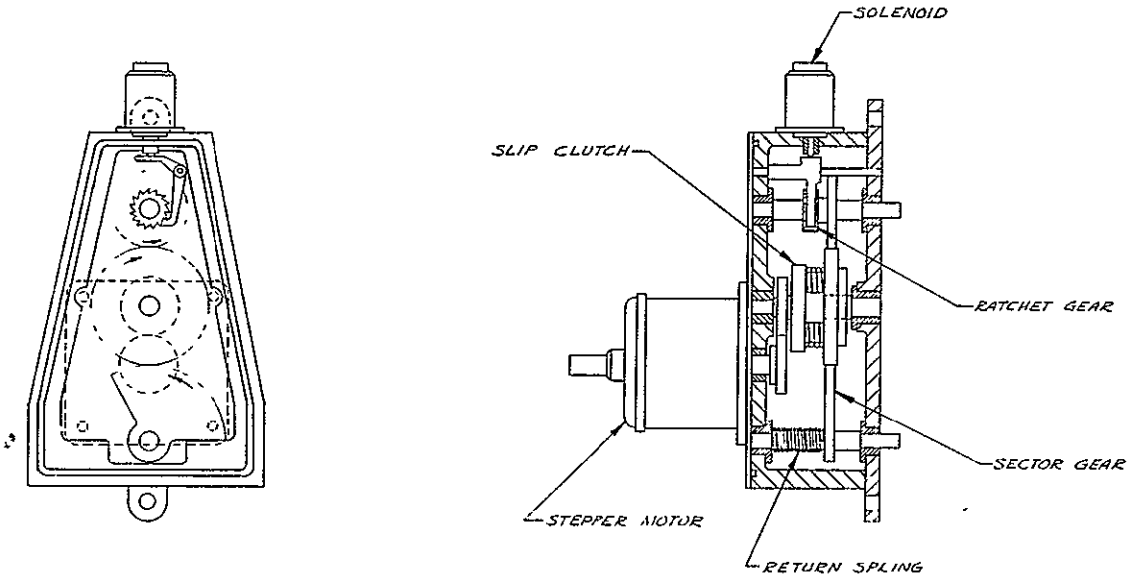

Figure 10 Cone Cover Actuator

Material for the spur gears will be 24 ST aluminum anodized and coated with a film of MoS_2. The shafts will be 410 stainless mounted in sleeve bearings of Rulon-A. Both the shafts and bearings will be covered by a film of MoS_2.

6.3 Anti-Frost Enclosures

Anti-frost enclosures are depicted in Figure 11. They are shown as part of the detector-optical assembly. Each enclosure consists of a cone of polyimide (or other suitable) film which encases the optical patch from the patch to the cone to prevent outgassing vapors from condensing on the patch optics. The conical enclosure will be provided with two tubes. One tube will be a charging tube which will allow the enclosure to be charged with one atmosphere or more of a very dry gas of high molecular weight (such as nitrogen). The other tube will be an open tube of very large ℓ/d ratio (approximately 1000 or greater). The tubing of large ℓ/d will allow the pressure to balance in the enclosure but because of the extreme slenderness of the tubing, molecular migration of gas or vapor through the tube will take an extremely long time. The time needed to exhaust the enclosure to a pressure at which gaseous thermal conductance is negligible ($\sim 10^{-4}$ Torr) can be set equal to the period of major instrument and spacecraft outgassing (~10 days). At the end of this period, the cone cover can be opened to permit operation of the cooler.

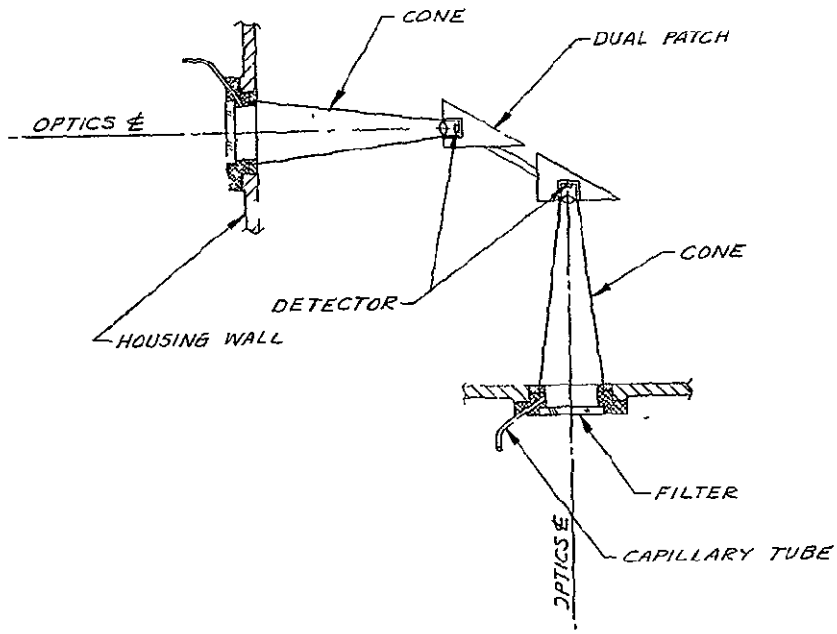

Figure 11 Anti-Frost Enclosures Attached to Dual Patch Assembly

7.0 TEST PLAN

Testing of the radiant cooler must provide for the simulation of the in-orbit environment. Specifically, we must furnish:

a. A low residual gas pressure or vacuum.

b. A black heat sink representative of the cold regions of space.

c. Thermal loads equivalent to those from the spacecraft and the earth.

In addition, means must be provided for measuring the temperatures of the cooler parts. A vacuum chamber will be used to provide the low residual gas pressure. The chamber to be used has an average pressure in the space above the experimental package of about 4×10^{-7} Torr after cryopumping. The cold space target will consist of a high conductivity copper structure cooled by a Norelco A-20 helium refrigerator. Cold structures of this type have been used on Contracts NAS5-10113 and NAS5-10491 to attain temperatures of 30 K and less. The thermal load from the earth will be simulated by a heater attached to the cone walls that would absorb emitted infrared and reflected solar energy from the earth. The thermal load from the spacecraft will be simulated by attaching the outer housing of the cooler to a heat sink in the form of a temperature regulated baseplate. The temperatures of the cooler parts (shield, cone structure, and two patches) will be measured by means of calibrated platinum resistance thermometers and the temperature gradients within the larger parts (shield and cone structure) by means of chromel-constantan differential thermocouples.

The installation of the radiant cooler in the test chamber is shown in Figure 12. The space reference (target) will be machined from electrolytic tough pitch copper (alloy No. 110) with the inside surface serrated (30 degree v-grooves) and painted with 3 M velvet coating No. 101-C10 black. The target will be protected against radiative inputs from the surroundings by a liquid nitrogen cooled shroud. The shroud will be a dip brazed assembly of 6061-T6 aluminum alloy. The outside surface will be covered with 3/8 inch diameter tubing for liquid nitrogen passage and the inside will be painted with 3 M velvet coating No. 101-C10 black. Both target and shroud will be suspended from the chamber wall by means of stainless steel aircraft cable. The target will be coupled to the helium refrigerator with a 1-3/4 inch diameter copper rod, and the shroud will be fed liquid nitrogen through vacuum fittings connected to a reservoir.

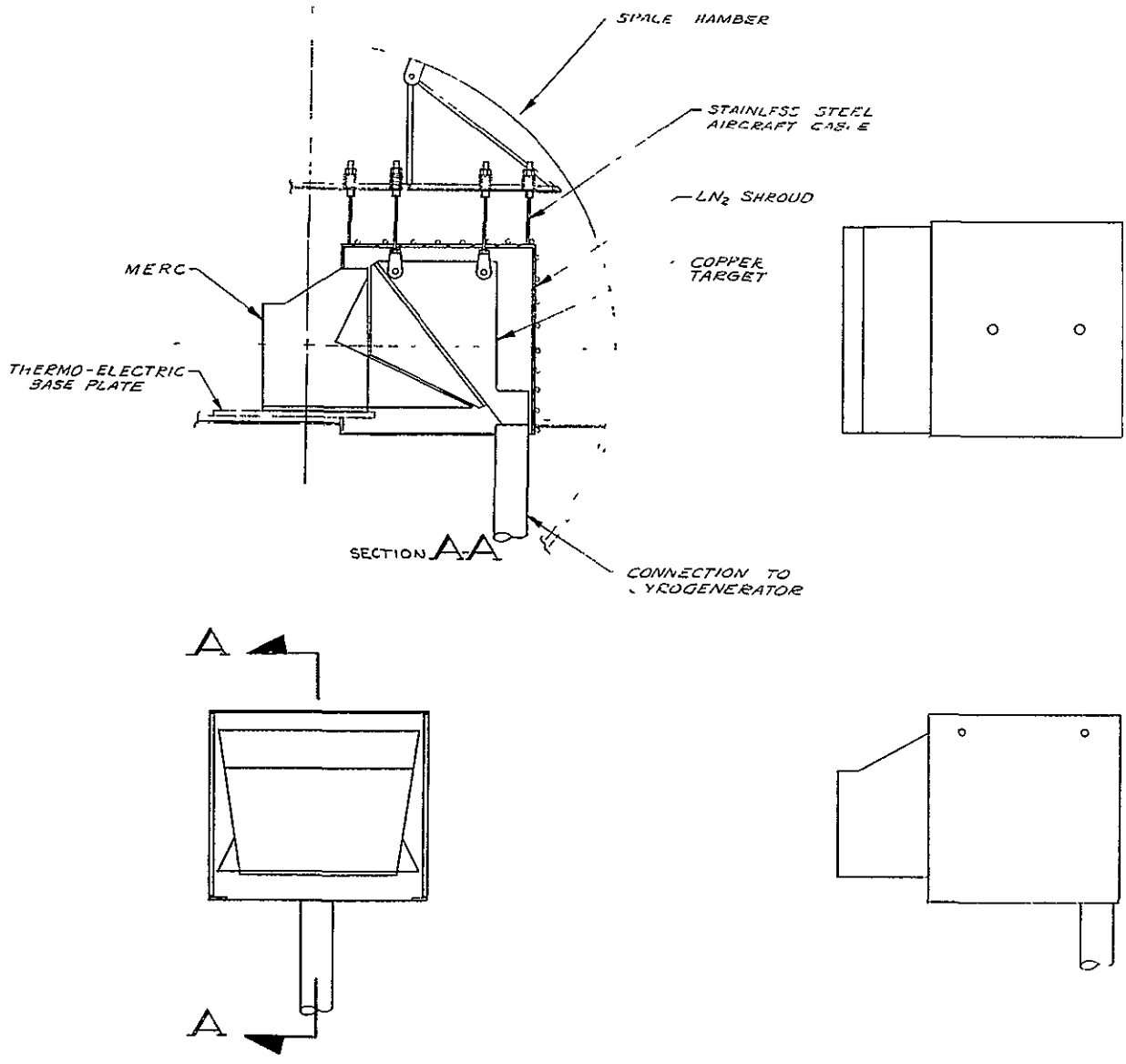

Figure 12 Space Chamber Installation

The cold space target is shown in Figure 13. The side plates are 3/8 inch thick, the face plate 1/2 inch, and the support plate 1 3/4 inches. The choice of electrolytic tough pitch (ETP) rather than OFHC (oxygen free) copper was made for the following reasons:

a. ETP is more readily available.

b. There will be no welded or brazed connections on the cold reference.

c. Thermal conductivity of ETP is close to that of OFHC, i.e., 14 watts/cm K for ETP and 12 watts/cm K for OFHC in the vicinity of 30 K.

ETP copper contains some oxygen, so that porosity free welds are difficult to make.

The temperature distribution in the cold space reference was calculated by the method described in the First Quarterly Report on Contract NAS5-10113 (Appendix XII) with the following assumptions:

a. The heat flux on the reference target is uniform.

b. The cooler provides a thermal load of 30 watts.

c. Shielding around the complete target assembly is maintained at 77 K so that the radiative transfer contribution from the surroundings is negligible.

The temperature drop across any length of the target is given by

$$\Delta\theta = Q\left(\frac{L}{KA} + \frac{I}{hA_o}\right)$$

where Q = thermal load

L = length of copper

A = cross-sectional area through which heat flows

K = thermal conductivity of copper

h = heat transfer coefficient through interface.

A_o = area of interface.

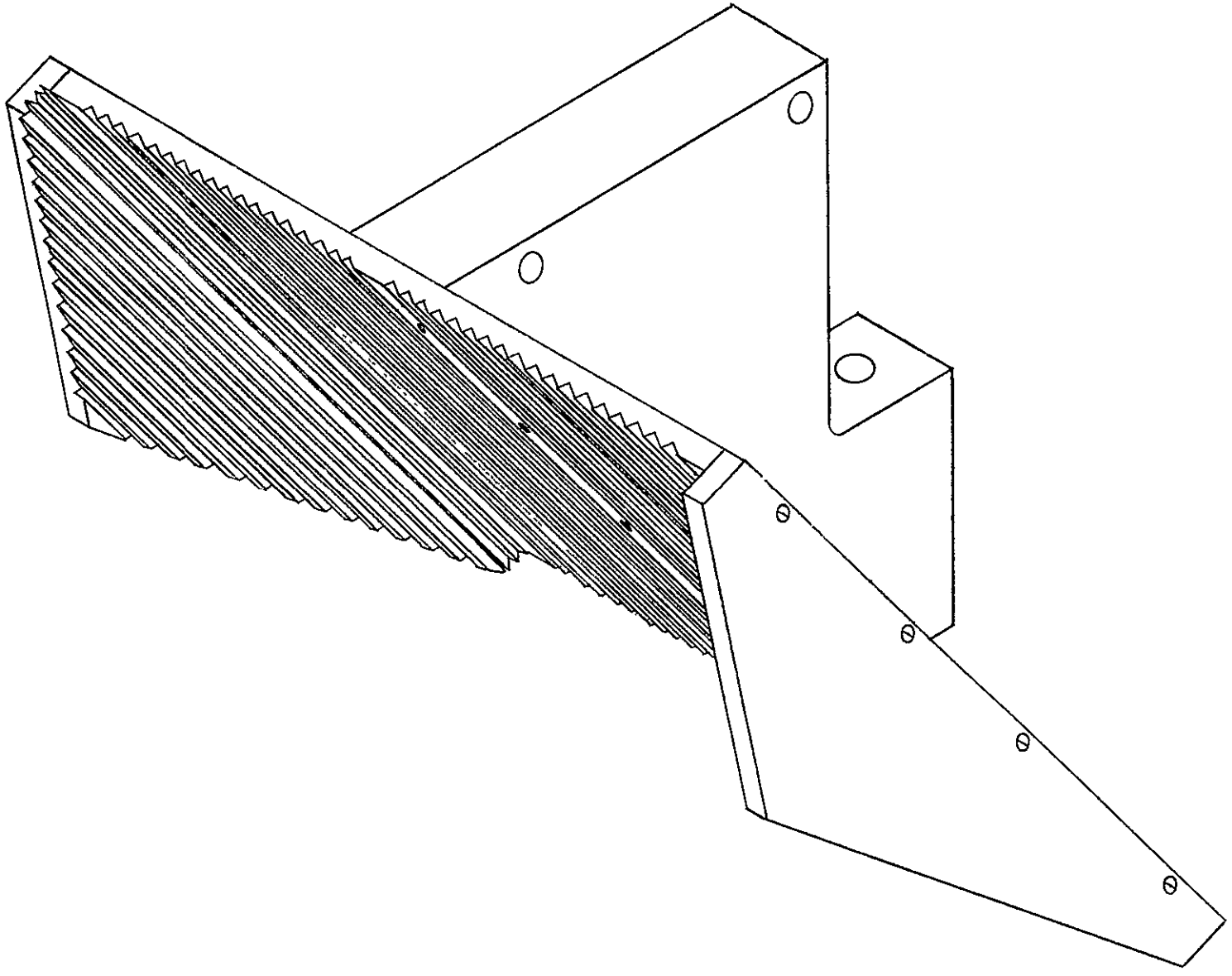

Figure 13 Cold Space Target

All interfaces are through silicone grease, for which $1/h = 0.3\ cm^2K/watt$. Starting at the end of one side plate and going to the center of the face plate we have:

$Q = 15$ watts, $L = 10.63$ in, $K = 35$ wats/in K

$A = 1.3\ in^2$, $A_o = 3.8\ in^2$, $1/h = .045\ in^2$ K/watt,

and $\Delta\theta = 15\ \frac{10.63}{(35)\ (1.3)} + \frac{.045}{3.8} = 3.7$ K.

From the center of the face plate through the support plate to the end of the support rod: $Q = 30$ wats, $L = 12$ inches, $K = 35$ watts/in K, $A = 21\ in^2$, $A_o = 21\ in^2 + 2.4\ in^2 = 23.4\ in^2$, $1/h = .045\ in^2$ K/watt, and

$$\Delta\theta = 30\ \frac{12}{(35)\ (21)} + \frac{.045}{23.4} = 0.55\ K$$

From the top end of the support rod to the end fastened to the cryogenerator: $Q = 30$ watts, $L = 20$ inches, $K = 35$ watts in ^oK, $A = 2.4\ in^2$, $A_o = 2.4\ in^2$, $1/h = .045\ in^2$ K/watt, and

$$\Delta\theta = 30\ \frac{20}{(35)\ (2.4)}\ \frac{.045}{2.4} = 7.7\ K$$

The temperature drop from the cryogenerator to the side plates of the reference target is then $3.7 + 0.6 + 7.7 = 12.0$ K. The temperature of the cold exchanger is about 15 K at the thermal load of 30 watts. The outer edge of the cold reference is then about 27 K.

The non-zero value of cold target temperature T_o adds a load $(1 - \epsilon_{pc})\ \sigma A_p T_o^4$ to the radiant cooler patch (Section 4.0). Because ϵ_{pc} is much less than unity, this is very nearly $\sigma A_p T_o^4$. The resultant increase in the temperature of the second patch for nominal values of the radiative properties (Table 25) is less than 0.2 K for all designs.

The thermal load from the spacecraft will be simulated by mounting the cooler on a temperature regulated baseplate. Cooler temperatures will be recorded at baseplate (instrument housing) temperatures of 0, 25, and 50 degrees C. The baseplate is heated and cooled by means of thermoelectric elements operating from a water cooled heat sink. An automatic controller regulates the temperature within the range from -15 degrees C and +60 degrees C to ±0.5 degrees C or better.

The thermal load from the earth will be simulated by means of a heater attached to the cone walls that would absorb the radiation. The load is in the vicinity of 0.1 watt (Section 3.0). Even for the design with the least earth shading (IIIA) this is only about 10 percent of the total load on the cone. As a result, a highly accurate simulation of the earth load is not needed for accurate cooler testing. The cooler will be tested with thermal loads on the patches corresponding to those produced by the introduction of the detector arrays. Thus the optical openings to the instrument housing, including the patch and cone windows (Appendix B), will be provided together with the necessary electrical leads (Section 3.0 and 4.0). The bias on the 90 K detector array will be simulated by the joule heating of a resistor.

The temperature ranges of the platinum resistance thermometers to be used in measuring cooler temperatures are listed in Table 43 together with the corresponding accuracies. Errors in the temperature measurements originate in the platinum sensors, their bridges, and in the bridge readout instrument. The output from all bridges covers the range from 0 to 50 mv for the temperature ranges shown. All sensors except that on the second patch will therefore produce outputs exceeding 10 mv.

Table 43. Temperature Measurement Ranges and Errors

		Errors		
Cooler Part	Range	Sensor-Bridge	Readout	Total *
Housing	0 to 100°C	±0.11°C	±0.05°C	±0.16°C
Cone	-150 to -50°C	±0.14°C	±0.05°C	±0.19°C
Patch 1	-200 to -100°C	±0.14°C	±0.05°C	±0.19°C
Patch 2	-200 to -100°C	±0.14°C	±0.02°C	±0.16°C

* Maximum

The integrating digital voltmeter used as a readout divice is a Doric Scientific Corporation (San Diego, California) Model DS-100-K6. The repeatability, accuracy and temperature effects for the two ranges of interest are listed in Table 44.

8.0 NEW TECHNOLOGY

The dual patch arrangement within the multi-element radiant cooler is considered new technology according to NASA Form 1162. The space allocated to the patch or volume containing the cooled components is divided into two parts. This permits the operation of two different detector arrays at two distinct temperatures. The individual temperatures can then be adjusted for optimum operation of each detector type. The dual patch mechanical assembly and its suspension system are illustrated in Figure 8 and 9 in Section 6.0.

A dual patch cooler could be obtained by designing both patches for the lower of the two temperatures and then intentionally increasing the temperature of one patch, e.g., by a greater conductive coupling to the cone structure. However, the lower temperature patch in the design described in this report has a significantly lower radiative coupling to the cone (see Sections 4.2 and 5.0) and therefore, an inherently lower temperature. This is a consequence of the cooler design and therefore of the spacecraft orbit and the available view to cold space (Section 1.0). Moreover, the lower temperature patch is suspended from the higher temperature patch rather than from the cone structure. As a result, the dual patch configuration may be considered a modification of the previously developed two-stage radiant cooler (Contract NAS5-10113, Final Report dated December 1967). Positioning of the second or lower temperature patch in a position of lower radiative coupling to the first-stage cone permits the elimination of the second-stage cone used to block the view to the first-stage cone.

APPENDIX A

THERMAL CONDUCTANCE OF THE ANTI-FROST ENCLOSURE

The anti-frost enclosure provides a thermal conductance path between the patch and the cone structure. Its thermal conductance may be obtained from that of a cylindrical disk. If a portion of the disk is cut along two radii that include and angle ϕ (Figure A-1), it can be rolled to form the truncated circular cone of the enclosure. Moreover, the thermal conductance is the same for both the partial disk and cone enclosure because the cuts are along boundaries across which no heat flows.

The thermal conductance of the partial disk is a fraction $\frac{\phi}{2\pi} = \tan \Theta$ of the complete disk, where Θ is the half angle of the cone enclosure. The thermal conductance of the enclosure is therefore given by (See, for example, J. M. Cork, Heat, Wiley, 1942, p. 129).

$$K_C = \frac{2 \pi k \delta \tan \Theta}{\ell n\left(\frac{r2}{r_1}\right)} \tag{A-1}$$

where k = thermal conductivity

δ = thickness of disk

r_2 = outside disk radius

r_1 = inside disk radius

This result may be obtained directly from the fact that the heat flux (power) across any cross-sectional area A of the truncated cone enclosure is constant and given by

$$P = k A \frac{dT}{d\ell}, \tag{A-2}$$

where ℓ is measured along the cone surface. The cross-sectional radius of the cone is

$$\rho = \ell \sin \Theta , \tag{A-3}$$

so that

$$A = \frac{2 \pi \rho \delta}{\sin \Theta} = 2 \pi \ell \delta \tan \Theta \tag{A-4}$$

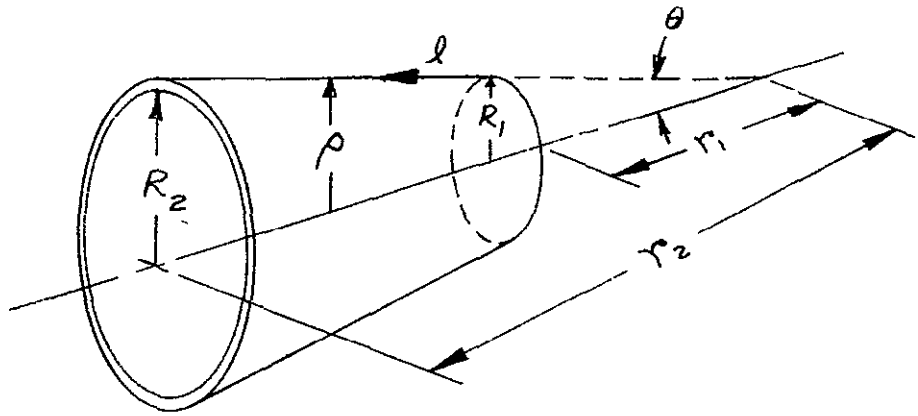

CONE

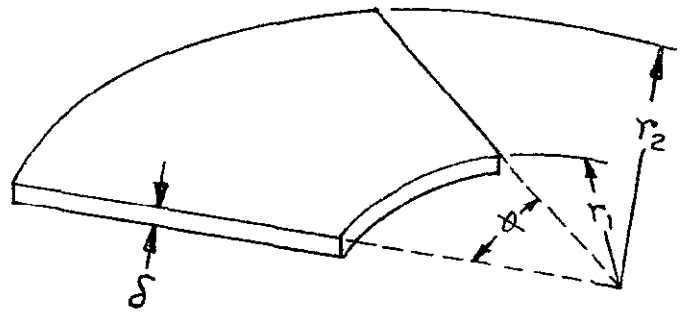

PARTIAL DISK

Figure A-1 Conical Enclosure and Its Equivalent Partial Disk

and the first term of the expansion, the thermal conductance becomes

$$K = \frac{\pi k \delta (R_2 + R_1)}{(r_2 - r_1)} \qquad \text{(A-12)}$$

This is the formula for a cylindrical enclosure of length $(r_2 - r_1)$, thickness δ, and radius $(1/2)(R_2 + R_1)$. The thermal conductance of the conical enclosure is therefore approximately that of a cylinder whose radius is the average cone radius. The relative error to this approximation is nearly

$$\epsilon = \frac{1}{3}\left(\frac{R_2 - R_1}{R_2 + R_1}\right)^2 \qquad \text{(A-13)}$$

We then have

$$P = 2 \pi k \ell \delta \tan \Theta \frac{dT}{d\ell} \tag{A-5}$$

Observing that

$$\frac{d\ell}{\ell} = \frac{dr}{r} , \tag{A-6}$$

this becomes

$$P \frac{dr}{r} = 2 \pi k \delta \tan \Theta \cdot dT \tag{A-7}$$

Integrating from r_1 to r_2 and T_1 to T_2, we obtain

$$P \ell n\left(\frac{r_2}{r_1}\right) = 2 \pi k \delta \tan \Theta (T_2 - T_1) \tag{A-8}$$

The thermal conductance is therefore

$$K = \frac{P}{T_2 - T_1} = \frac{2 \pi k \delta \tan \Theta}{\ell n\left(\frac{r_2}{r_1}\right)} \tag{A-9}$$

The logarithm may be expanded according to

$$\ell n X = 2\left[\frac{X-1}{X+1} + \frac{1}{3}\left(\frac{X-1}{X+1}\right)^3 + \cdots\right] , \tag{A-10}$$

where

$$X = \frac{r_2}{r_1} = \frac{R_2}{R_1}$$

and R is the cone cross-sectional radius corresponding to the disk radius r. Using

$$\tan \Theta = \frac{R_2 - R_1}{r_2 - r_1} \tag{A-11}$$

APPENDIX B

RADIATIVE INPUT THROUGH AN OPTICAL OPENING

The magnitude of the radiative input (Φ_o) to a patch through an optical opening depends on the optical and mechanical design of the instrument. A typical arrangement is shown in Figure B-1. The filter window at the edge of the patch views a black window on the cone structure and black multilayer insulation (seen edge on through the anti-frost enclosure) between the cone and patch. The cone window is selected to block radiation from components beyond it in the direction of the instrument housing. The window also serves two other purposes. It provides the seal for both the anti-frost enclosure and for the cone enclosure. The cone enclosure is sealed to prevent outgassing of the instrument through the cooler and possibly also to permit its evacuation during bench cooling of the detector.

A good choice of cone window for the 90 K (Hg Cd Te) patch is Irtran 2, which absorbs or reflects radiation at wavelengths of 15 μm and greater (D. E. McCarthy, Appl. Opt. 2, 591, 1963). In combination with a germanium patch window, especially if the germanium is coated to reject (by reflection) radiation at lower wavelengths, the window essentially eliminates radiative coupling between the patch and objects beyond the window. Moreover, as shown below, the view factor from the patch to the cone window is very small. For the 120 K (InAs) patch, a sapphire cone window can be used. Sapphire reflects or absorbs all radiation beyond about 7 μm (D. E. McCarthy, Appl. Opt. 4, 317, 1965).

The value of Φ_o is then given by

$$\Phi_o = \sigma \epsilon_o A_o \left[F_{ow} T_w^4 + \left(1 - F_{ow}\right) T_i^4 \right] , \qquad \text{(B-1)}$$

where

A_o = area of opening on patch

ϵ_o = infrared absorptance plus infrared transmittance of patch filter window

F_{ow} = view factor from A_o to cone window

T_w = temperature of cone window

T_i = average radiation temperature of insulation between cone and patch

The insulation temperature is approximately $T_i^4 = \frac{1}{2} T_c^4$, so that we have

$$\Phi_o = \frac{1}{2} \sigma \epsilon_o A_o T_w^4 (1 + F_{ow}). \quad \text{(B-2)}$$

The view factor from the patch opening to the cone window is set by the optical design and given approximately by

$$F_{ow} = \frac{1}{4 f_n 2} \quad \text{(B-3)}$$

where f_n is the f-number of the optical beam between the cone and patch. For a typical instrument, the instantaneous geometric field of view ϕ is 1×10^{-4} radian and the entrance aperture diameter D, 10 inches. A detector element whose sensitive area is s inch on a side then requires an f-number (at the detector) of

$$f_n = \frac{S}{\phi D} . \quad \text{(B-4)}$$

The f-number between the cone and patch is equal to or larger than this value. For s in the range from 2×10^{-3} to 10×10^{-3} inch, f_n is from 2 to 10. As a result, F_{ow} is typically much less than unity, and the equation for the radiative input becomes

$$\Phi_o = \frac{1}{2} \sigma \epsilon_o A_o T_w^4 \quad \text{(B-5)}$$

A germanium patch window has a reflectance of about 0.4 over a wide wavelength range. A sapphire patch window reflects an average of about 0.4 at wavelengths above 11 μm, a region that includes most of the blackbody radiation for source temperature between that of the cone and patch. Thus for either patch, ϵ_o is about 0.6.

For a patch opening A_o of 0.4 inch diameter and a cone window temperature T_w of 165 K, the radiative input through the optical opening is then approximately

$$\Phi_o = 1 \times 10^{-3} \text{ W}.$$

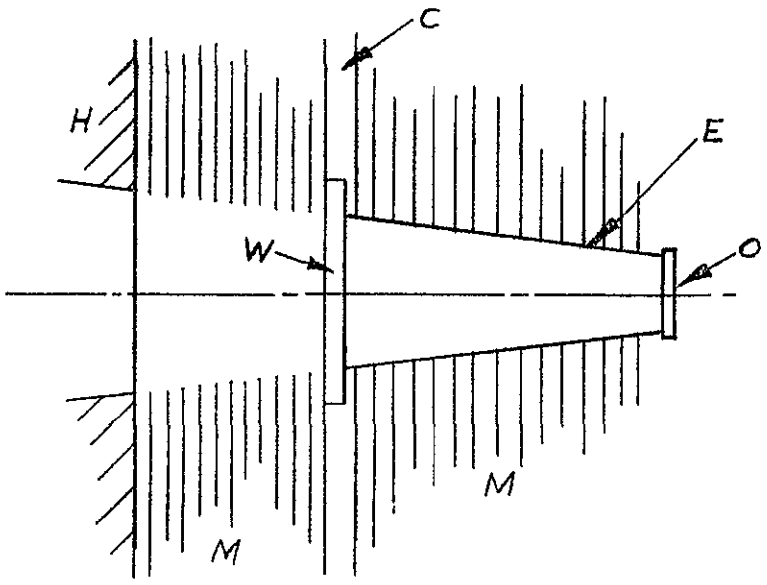

H = HOUSING
W = CONE WINDOW
O = PATCH WINDOW
C = CONE STRUCTURE
E = ANTI-FROST ENCLOSURE
M = MULTILAYER INSULATION

Figure B-1 Optical Opening Between Patch and Housing